


## Article

# Unveiling Valuable Geomechanical Monitoring Insights: Exploring Ground Deformation in Geological Carbon Storage

Gabriel Serrão Seabra <sup>1,2,\*</sup> , Marcos Vitor Barbosa Machado <sup>2,\*</sup> , Mojdeh Delshad <sup>3</sup> , Kamy Sepehrnoori <sup>3</sup>, Denis Voskov <sup>1,4</sup> and Femke C. Vossepoel <sup>1</sup>

<sup>1</sup> Faculty of Civil Engineering and Geosciences, Delft University of Technology, Stevinweg 1, 2628 CN Delft, The Netherlands; d.v.voskov@tudelft.nl (D.V.); f.c.vossepoel@tudelft.nl (F.C.V.)

<sup>2</sup> PETROBRAS, Rio de Janeiro 20231-030, Brazil

<sup>3</sup> Hildebrand Department of Petroleum and Geosystems Engineering, The University of Texas at Austin, Austin, TX 78712, USA; delshad@mail.utexas.edu (M.D.); kamys@mail.utexas.edu (K.S.)

<sup>4</sup> Energy, Science and Engineering Department, Stanford University, Stanford, CA 94305, USA

\* Correspondence: g.serraoseabra@tudelft.nl (G.S.S.); marcosbarbosa@petrobras.com.br (M.V.B.M.)

**Featured Application:** This study emphasizes the importance of comprehensive monitoring, calibration, and optimization of storage strategies in a saline aquifer. It also highlights the need to manage geomechanical risks and uncertainties. By understanding these risks and employing suitable monitoring techniques, the integrity and safety of GCS can be ensured, contributing to the reduction of CO<sub>2</sub> emissions.

**Abstract:** Geological Carbon Storage (GCS) involves storing CO<sub>2</sub> emissions in geological formations, where safe containment is challenged by structural and stratigraphic trapping and caprock integrity. This study investigates flow and geomechanical responses to CO<sub>2</sub> injection based on a Brazilian offshore reservoir model, highlighting the critical interplay between rock properties, injection rates, pressure changes, and ground displacements. The findings indicate centimeter-scale ground uplift and question the conventional selection of the wellhead as a monitoring site, as it might not be optimal due to the reservoir's complexity and the nature of the injection process. This study addresses the importance of comprehensive sensitivity analyses on geomechanical properties and injection rates for advancing GCS by improving monitoring strategies and risk management. Furthermore, this study explores the geomechanical effects of modeling flow in the caprock, highlighting the role of pressure dissipation within the caprock. These insights are vital for advancing the design of monitoring strategies, enhancing the predictive accuracy of models, and effectively managing geomechanical risks, thus ensuring the success of GCS initiatives.

**Keywords:** GCS; geomechanics; caprock; ground deformation monitoring; saline aquifer



**Citation:** Seabra, G.S.; Barbosa Machado, M.V.; Delshad, M.; Sepehrnoori, K.; Voskov, D.; Vossepoel, F.C. Unveiling Valuable Geomechanical Monitoring Insights: Exploring Ground Deformation in Geological Carbon Storage. *Appl. Sci.* **2024**, *14*, 4069. <https://doi.org/10.3390/app14104069>

Academic Editor: Nikolaos Koukoulas

Received: 5 April 2024

Revised: 8 May 2024

Accepted: 8 May 2024

Published: 10 May 2024



**Copyright:** © 2024 by the authors. Licensee MDPI, Basel, Switzerland. This article is an open access article distributed under the terms and conditions of the Creative Commons Attribution (CC BY) license (<https://creativecommons.org/licenses/by/4.0/>).

## 1. Introduction

Scenarios considered by international entities, such as the International Agency (IEA), point out the complexity of actions needed to achieve the goals established for reducing emissions of Greenhouse Gases in the coming decades, simultaneously with the desired transformation in energy generation sources. The report “World Energy Outlook 2022” [1] emphasizes that multiple technologies and energy sources will play an essential joint role in providing energy resources for the planet in a more sustainable scenario. Among the various options for reducing CO<sub>2</sub> emissions, Carbon Capture and Storage (CCS) presents itself as a technology with significant potential to reduce CO<sub>2</sub> emissions in a (probable) scenario of continued use of fossil fuels in the coming decades.

A CCS project involves CO<sub>2</sub> capture from high-emission industries and injecting it into geological formations, such as aquifers and depleted hydrocarbon reservoirs. One of the most critical barriers to long-term and large-volume CO<sub>2</sub> storage in geological formations

is proof of safe and reliable storage. For that, CO<sub>2</sub> can take advantage of different trapping mechanisms in porous media [2–5]; for example, free CO<sub>2</sub> migration is controlled by the structural and stratigraphic trapping exerted by the caprock during the short term, encompassing the injection time, known as a primary mechanism. During this stage, the caprock plays an essential role in the security of the geological storage operation due to CO<sub>2</sub>'s buoyancy, which can move it up to the surface in onshore fields or the seafloor in the case of offshore storage sites. In the Frio CO<sub>2</sub> field demonstration project conducted in the U.S. [6], CO<sub>2</sub> was injected in a deeper zone below several well-known shale seals. However, some authors [7] are currently reviewing the need for a caprock to control the plume rising because (i) there is no prescriptive regulation concerning geologic seals and (ii) a composite confining system, e.g., a set of discontinuous barriers, can create long and tortuous paths that attenuate the mobile CO<sub>2</sub> saturation.

During the mid and long term, part of that mobile CO<sub>2</sub> will be dissolved in water (solubility trapping) as time passes, especially in low-salinity brine under high-pressure and low-temperature conditions [8,9]. Molecular diffusion and brine solubility are the main physical phenomena that facilitate the dissolution of CO<sub>2</sub> into a brine. As CO<sub>2</sub> dissolves into saline water, the density of the resulting CO<sub>2</sub>-dissolved brine increases. This density difference between the CO<sub>2</sub>-dissolved brine and pure brine leads to the sinking of the denser CO<sub>2</sub>-dissolved brine, while the pure brine rises [10,11]. Density-driven convective mixing accelerates the rate of mass transfer of CO<sub>2</sub>, promotes its dissolution, and enhances the stability and safety of the geological storage [12–14].

In addition to the solubility trapping, saturation changes caused by the rising plume can lead to more CO<sub>2</sub> being trapped as a residual phase due to relative permeability and capillary hysteresis [15–17]. On saline aquifers, thermally enhanced dissolution of the CO<sub>2</sub> occurs [18]. Beyond that, in a few cases, some CO<sub>2</sub> can be trapped as minerals because of the resulting pH of the brine and the mineralogy of the rock [19,20]. Therefore, those additional mechanisms increase storage security when the buoyant CO<sub>2</sub> is immobile in the pore space or no longer exists as a free phase (generally, as supercritical CO<sub>2</sub>).

Geological CO<sub>2</sub> storage also involves a range of geomechanical risks associated with associated physical phenomena. These risks arise from the interaction between the injected CO<sub>2</sub> and the geological formations, leading to changes in rock mechanics, fluid dynamics, and chemical reactions. Key concerns include induced seismicity due to subsurface stress alterations, caprock integrity challenges from pressure-induced deformation, and changes in rock and fault strength owing to CO<sub>2</sub>-related geochemical reactions. Furthermore, the integrity of wells is at risk due to CO<sub>2</sub> corrosion, and the long-term effects of mineral dissolution or precipitation add complexity to the stability and safety of storage sites [21]. Among these, excessive ground displacement emerges as a critical issue. For onshore projects, such ground displacement can lead to considerable damage to houses and buildings, as in the case of the Groningen gas field in The Netherlands [22]. In offshore environments, the primary concern lies with the impact on subsea infrastructure and surface facilities, such as the Ekofisk oil field in the North Sea [23], where substantial subsidence led to significant engineering interventions to mitigate the adverse effects. This paper specifically focuses on ground deformation as the principal risk under investigation.

During the injection process and even afterward, the injection of large volumes of CO<sub>2</sub> into deep geological formations can cause significant pressure buildup and change stresses on the reservoir and the surrounding rocks. The pressure buildup induced by fluid injection can lead to expansion of the storage formation in proportion to the pressure increase. This expansion pattern can cause an uplift of the caprock, as observed in some actual GCS projects [24,25]. Additionally, the dissolution of CO<sub>2</sub> into water forms carbonic acid, which lowers the pH and can result in the dissolution of rock. Furthermore, vaporization of water can also lead to the precipitation of minerals [26–29]. These geochemical reactions have the potential to alter the geomechanical properties of rocks and faults, which depends on the position of the displacement fronts [30,31]. Therefore, injection conditions that may initially appear geomechanically stable could become unstable in the long term if geochemical

reactions weaken the strength of the rocks or faults [32]. Furthermore, in the event of fault reactivation, induced seismicity is possible, which has been associated with the risk of generating seismic activity due to stress changes caused by CO<sub>2</sub> injection [33,34].

In the pursuit of advancing GCS technologies, the importance of conducting comprehensive uncertainty analyses on key geomechanical parameters cannot be overstated. These analyses are essential for accurately characterizing the behaviors of geological formations under CO<sub>2</sub> injection scenarios. The variability inherent in rock properties, coupled with the dynamic nature of CO<sub>2</sub> injection processes, introduce uncertainties that must be addressed to ensure the efficacy and safety of CO<sub>2</sub> sequestration efforts. By evaluating the sensitivity of model outcomes to changes in rock mechanical properties, caprock permeability, and injection rates, researchers can identify critical thresholds and optimize monitoring and mitigation strategies. For instance, a study [35,36] on sensitivity analysis of geomechanical constraints in CO<sub>2</sub> storage highlights the significant impact of rock properties and injection rate on pressure buildup and CO<sub>2</sub> plume migration, underscoring the importance of accurately characterizing these parameters to predict storage site performance. Similarly, work on minimizing geomechanical risks under geological uncertainty through controlled CO<sub>2</sub> injection into storage reservoirs [37] demonstrates the critical role of understanding and managing uncertainties in geomechanical properties to ensure caprock integrity and minimize leakage risks. Moreover, a study [38] on the long-term effects of CO<sub>2</sub> sequestration on rock mechanical properties further illustrates the potential changes in rock integrity over time due to CO<sub>2</sub>-rock interactions, highlighting the need for long-term monitoring and model calibration to account for these changes. The research [39] on uncertainty and global sensitivity analysis of CO<sub>2</sub> storage capacity prediction in deep saline aquifers also emphasizes the importance of identifying and managing key uncertainties in geomechanical and other parameters to ensure accurate storage capacity estimates and safe CO<sub>2</sub> sequestration.

In the context of modeling vertical displacements due to reservoir activities, various monitoring technologies offer distinct advantages and limitations. High-precision tiltmeters are a method for monitoring direct surface deformation in onshore and offshore targets. With an accuracy equivalent to detecting an uplift of 0.01 mm over a typical distance of 10 km, tiltmeters provide precise measurements of ground surface movement [5], especially for subsidence mapping purposes in hydrocarbon fields or aquifers due to groundwater removal [40]. Fiber Optic Sensing Technology offers high-resolution, continuous deformation profiles over long distances, making it suitable for detailed spatial mapping in both onshore and offshore fields. Other methods are most likely to be applied to onshore fields, like Interferometric Synthetic Aperture Radar (InSAR), which excels in monitoring large areas with millimeter accuracy, though its application is limited offshore or in dense forests. The Global Positioning System (GPS) provides three-dimensional displacement data, which are crucial for comprehensive movement analysis across both local and regional scales. Laser Scanning (LiDAR) generates precise topographical models, aiding in the detection of subtle ground deformations. Each method contributes uniquely to the comprehensive monitoring and analysis of ground movement, enabling a more nuanced understanding of the geomechanical effects of reservoir activities [25]. A typical lower boundary used for ground displacement detection is 1 mm/year [41]. By providing precise measurements of ground surface movement, these monitoring methods enable the use of ground deformation as a surface tool to monitor the redistribution of CO<sub>2</sub> and the diffusion of pressure into the subsurface. In this context, the primary objective of this study is to assess the technical feasibility of the proposed idea by employing a comprehensive numerical simulation framework that combines fluid flow and geomechanics in an offshore reservoir case study. Therefore, the objectives of this study can be described as follows:

- a. Study the ongoing dissipation of pressure in the reservoir even after the CO<sub>2</sub> plume has stabilized;
- b. Analyze the continued ground deformation due to CO<sub>2</sub> movement and pressure dissipation after the cessation of CO<sub>2</sub> injection;

- c. Investigate how the uplift behavior can be utilized for long-term monitoring of CO<sub>2</sub> redistribution;
- d. Provide technical arguments supporting the feasibility of monitoring the ground uplift caused by CO<sub>2</sub> storage in offshore targets, even after the injection has ceased;
- e. Examine the role of uplift in monitoring scenarios where the CO<sub>2</sub> plume is confined but the pressure continues to dissipate;
- f. Conduct sensitivity analyses on geomechanical properties and injection rates to enhance the conclusions of our base case.

The concept of modeling surface deformation data to monitor CO<sub>2</sub> storage activity in porous media is not new. It has been successfully demonstrated in projects like the In Salah CCS project in Algeria, where the geomechanical response at the ground surface to subsurface CO<sub>2</sub> injection was effectively reproduced using a coupled reservoir simulation–geomechanical model [24,42]. However, it is worth noting that in their study, the authors relied on interferometric synthetic–aperture radar (InSAR) data to calibrate the numerical model [41,43]. In contrast, our approach aims to validate the feasibility of directly measuring ground uplift as a monitoring tool beyond the InSAR data, which are restricted to onshore and no covered areas. This research seeks to contribute to the advancement of the field by exploring a supplementary method that can potentially offer more cost-effective and accessible monitoring solutions. This also has potential to aid in accurately determining the optimal placement of the monitoring instrument within the so-called Area of Review. The Area of Review is a regulatory term that encompasses the storage site, focusing on the edges of the injected CO<sub>2</sub> plume and areas of elevated pressure [44,45]. It necessitates a monitoring strategy informed by a deep understanding of the geomechanical state of the reservoir, rather than assumptions based on the CO<sub>2</sub> injection locations alone. By incorporating robust geomechanical analyses, we can optimize the surveillance of CO<sub>2</sub> sequestration sites, thereby enhancing the fidelity of monitoring systems and maintaining the integrity of long-term carbon storage solutions. This, in turn, can support the exploration of alternatives, such as drilling new wells to produce brine, to relieve the pressure buildup associated with such surface events [46,47]. The technical evidence to be explored in this study will also provide new insights into the magnitude of geomechanical events and their occurrence timeframe, supporting the application of several ground deformation monitoring tools for GCS.

The following aspects are outside the scope of this paper:

- Accurately representing of enhanced CO<sub>2</sub> dissolution at the reservoir scale, as performed by [18,48,49]. This assumption is based on the fact that the gridblocks used in our coupled geomechanics and numerical flow simulations may not accurately capture the dissolution of CO<sub>2</sub> in brine. Our study primarily focuses on ground deformation; therefore, a simplified representation of the dissolved CO<sub>2</sub> was adopted to enable the simulation of a field-scale model. This model encompasses the caprock and the surrounding rocks, allowing for a comprehensive sensitivity analysis regarding the geomechanical properties.
- Consideration of impurities and free water content in the CO<sub>2</sub> stream injected.
- Modeling the dry-out effect due to water vaporization with CO<sub>2</sub> injection or another injectivity issue, which can be found in Machado et al. [50].
- CO<sub>2</sub> leakage through wells with poor cement jobs, as pointed out by Gholami et al. [51], which could be the most important reason for migration and leakage.
- Evaluating other monitoring techniques, such as time-lapse seismic surveys or micro-seismic methods.
- Evaluating data assimilation or inversion methods of ground displacements for CO<sub>2</sub> plume tracking.
- Modeling geochemical reactions between CO<sub>2</sub> and rock minerals, as performed by [52,53].
- Modeling caprock wettability changes.
- Modeling of fault activation and fracture propagation induced by CO<sub>2</sub> injection.

- Evaluating the impact of temperature on geomechanical behavior.
- Assessing small-scale rock microstructures influencing CO<sub>2</sub> migration and storage.

The paper is organized as follows. Section 2 describes basic petrophysical modeling for both sandstone and shale, which is important for the understanding of the geological context of the study area. Section 3 describes the modeling of CO<sub>2</sub> entrapment. Section 4 covers the geomechanical modeling of the CO<sub>2</sub> injection. Section 5 delves into the methodology and results, showcasing the numerical simulation outcomes and discussing the implications of the ground deformation phenomena observed. It also presents a sensitivity analysis to assess the impact on the geomechanical behavior of the reservoir and the caprock system with wide variations in parameters. Lastly, the paper is concluded by summing up the key findings and giving an overview of contributions that the study makes to the literature on GCS.

## 2. Petrophysical Modeling for Sandstone and Shale

The saline aquifer geological model in this study, including geometry and porosity/permeability distributions, was derived from a benchmark model, referred to as UNISIM-I [54]. It was constructed based on structural, facies, and petrophysical data obtained from the Namorado Oil Field in the Campos Basin, Brazil. The 3D model, including the over, lateral, and underburden, consists of 114 × 66 × 56 gridblocks with lateral dimensions of 170 × 170 m<sup>2</sup> and variable thickness (Figure 1), discretized using a corner point grid. Table 1 provides a summary of the mean values for key petrophysical properties assigned to the model.

The model represents a heterogeneous sandstone reservoir, and the associated siliceous shaly caprock was assumed to have homogenous properties, depicted in Table 1. The shale properties are typical for this type of rock [55,56]. Figure 1 shows the porosity distribution in the model. The low-porosity zone in blue represents the shale layers, and it highlights the area of the CO<sub>2</sub> injection well, positioned on a high-porosity lower flank of the reservoir. This specific positioning, a practice observed in GCS projects to optimize the injection [57,58], leverages gravitational forces to enhance CO<sub>2</sub> dispersion and retention within the high-porosity zones, thereby optimizing injection. The blue zones surrounding this area represent the shale layers with low porosity, serving as a caprock to contain the CO<sub>2</sub>. This placement is critical to ensure the containment of the CO<sub>2</sub> within the target zone. The left figure presents a 3D view of the geological model. The right figure provides a slice through the model, emphasizing the depth of the reservoir and allowing for a focused examination of the geological features and porosity at a specific subsurface level.

The dynamic properties used in this model are based on the characterization proposed by Machado et al. [59], and it will be discussed in the next paragraphs. The relative permeability curves for CO<sub>2</sub> and brine in sandstone and shale were obtained from Bennion and Bachu [60]. The CO<sub>2</sub>–brine capillary pressure curves were obtained from a J-function fitted to the data from Abdoulghafour et al. [61] for the sandstone and from Bennion and Bachu [62] for the shale. Figures 2 and 3 show the final drainage curves used in the simulation for the aquifers and their caprock, respectively. The imbibition curves are generated according to the hysteresis model, which is detailed in the next section.

**Table 1.** Summary of main petrophysical properties used in the geological model.

	Sandstone	Shale
Porosity ( $\phi$ )	0.20 (mean)	0.10
Permeability ( $k$ )	300 mD (mean)	0.001 mD
$k_v/k_h$ ratio	0.1	0.1
Pore compressibility	$5.8 \times 10^{-7}$ kPa <sup>-1</sup>	$5 \times 10^{-8}$ kPa <sup>-1</sup>
Young's modulus	1 GPa	10 Gpa
Poisson's ratio	0.25	0.30
Relative permeability	Figure 2	Figure 3
Capillary pressure	Figure 2	Figure 3

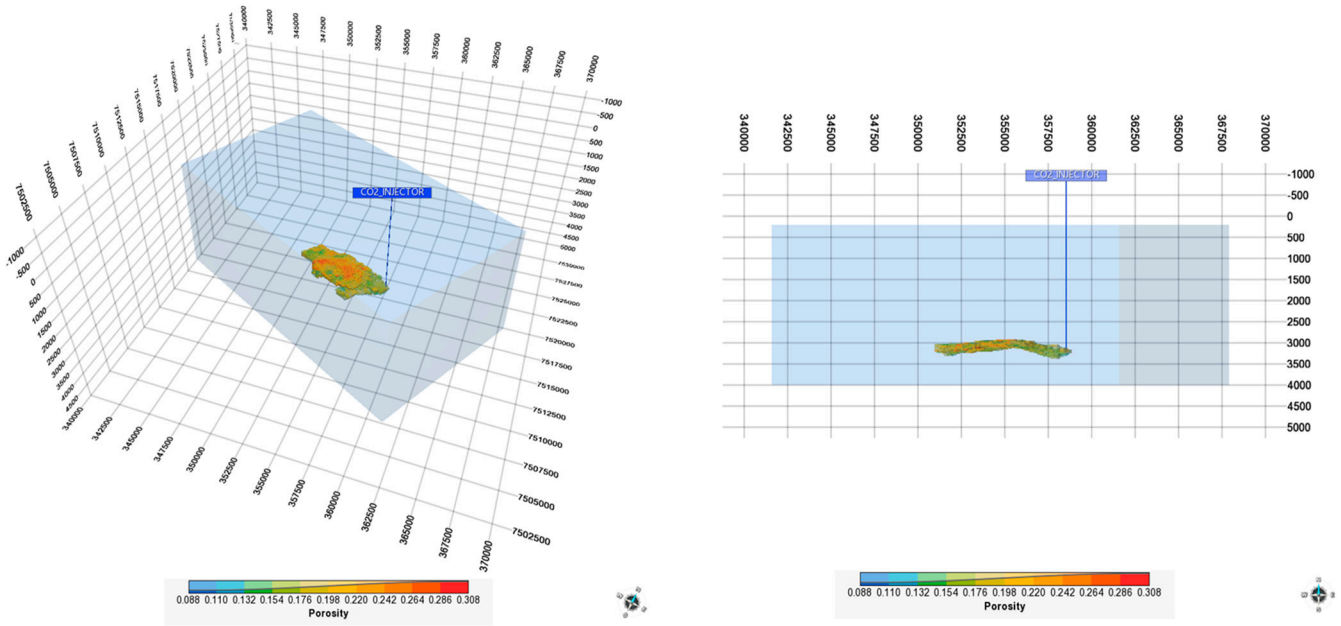


**Figure 1.** 3D view of the geological model showing porosity distribution and injector well position (left). A sliced view highlighting the depth of the reservoir and porosity characteristics (right). Coordinates are in meters.

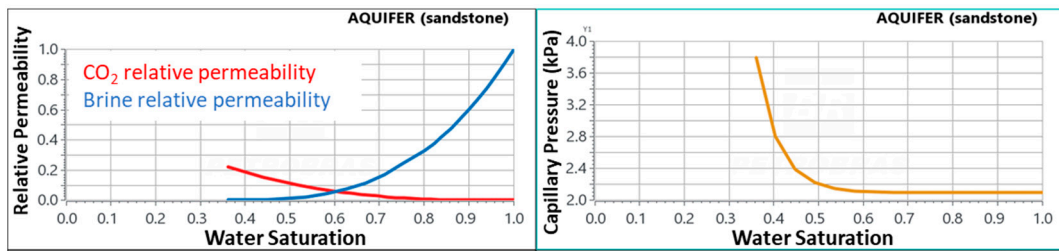


**Figure 2.** Drainage relative permeability (left) and capillary pressure ((right) in orange) for the sandstone.

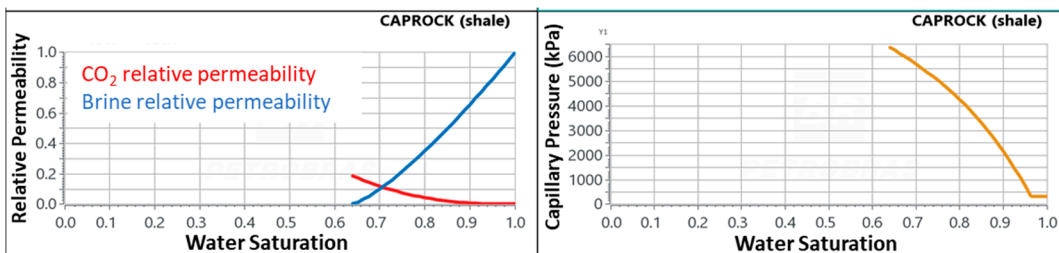


**Figure 3.** Drainage relative permeability (left) and capillary pressure ((right) in orange) for the shale caprock.

### 3. Modeling CO<sub>2</sub> Entrapment for Sandstone and Shale Formations

The sandstone saline aquifer and its shale caprock in the model in this study were numerically simulated using CMG-GEM [63]. CMG-GEM is known for its versatility and robustness in predicting and analyzing various thermodynamic properties and fluid behavior for GCS projects [2,3,16,50,64]. It is based on the discretization of component conservation and energy balance equations in space and time using finite volume and finite difference methods [65,66].

One of the key strengths of the CMG-GEM model lies in its accurate prediction of CO<sub>2</sub> phase behavior for wide ranges of pressure and temperature. It can effectively capture

the transition of CO<sub>2</sub> from gaseous to liquid states, as well as its behavior in supercritical conditions. Overall, the CMG-GEM simulation model enables accurate prediction and analysis of CO<sub>2</sub> behavior and the following trapping mechanisms:

- CO<sub>2</sub> solubility in brine is modeled in this study by applying the Li and Nghiem model [67]. This model has been calibrated using published experimental data, and it calculates Henry's constant based on Equation (1), which considers the pressure and temperature variations. Additionally, the impact of brine salinity on gas solubility in the aqueous phase is accounted for through the salting-out coefficient [68].

$$\ln(H_i) = \ln(H_i^*) + \frac{\bar{v}_i}{RT}(p - p^*) \quad (1)$$

where

$H_i$ : Henry's constant at current pressure ( $p$ ) and temperature ( $T$ );

$H_i^*$ : Henry's constant at reference pressure ( $p^*$ ) and temperature ( $T$ );

$\bar{v}_i$ : partial molar volume at infinite dilution;

$R$ : universal gas constant;

$i$ : species dissolved in water (CO<sub>2(aq)</sub> in this work).

The  $H_i^*$  constant was computed considering the initial conditions of the models in Table 2.

**Table 2.** Summary of the reference conditions applied to the solubility calculation in the aquifer models.

	Saline Aquifer
Reference pressure	11,800 kPa @ 1000 m
Temperature	80 °C
Salinity	50,000 ppm
$H_i^*$	$5.66 \times 10^5$

- Solubility trapping in brine can be enhanced through physical diffusion, which is mandatory for an accurate representation of the convective mixing to obtain a grid-converged solution. To model this effect, even in a simplified way due to our model's scale, the diffusion coefficient ( $D$ ) for supercritical CO<sub>2</sub> in brine is applied to compute the effective CO<sub>2</sub> diffusion ( $D_{eff}$ ) considering tortuosity  $\tau$  [69]:

$$D_{eff} = \frac{D}{\tau} \quad (2)$$

In shales, where diffusion is a relevant mechanism due to lower permeability, the tortuosity value ranges from approximately 40 to 70 [70]. An effective diffusion equal to  $2.8 \times 10^{-7}$  cm<sup>2</sup>/s [71] is used in the simulations.

- The residual CO<sub>2</sub> trapping due to the relative permeability and capillarity hysteresis with the saturation changes was modeled with the maximum gas trapped ( $S_{gt}$ ) converted to the Land's constant I [72] in the two-phase Carlson's model [73], according to Equation (3):

$$S_{gt} = \frac{S_{g \max}}{1 + CS_{g \max}} \quad (3)$$

where  $S_{g \max}$  is the maximum gas saturation.

Burnside and Naylor [74] obtained a  $S_{gt}$  distribution for sandstone, shale, and carbonates based on more than 30 published coreflood data for CO<sub>2</sub> and brine. The mean values for each lithology are presented in Table 3.

**Table 3.** Maximum gas trapped due to hysteresis of relative permeabilities and capillary pressure [65].

	Sandstone	Shale
$S_{gt}$	0.25	0.35

#### 4. Geomechanical Modeling of CO<sub>2</sub> Injection

As emphasized in the Introduction, the modeling of geomechanics for CO<sub>2</sub> injection in sandstone and shale formations is a critical aspect of ensuring the safety and efficacy of GCS projects. CMG-EM's Finite Element geomechanical coupling provides a sophisticated tool for analyzing the interactions between rock formations and the injected CO<sub>2</sub> [63]. This module relies on the fundamental principles of rock mechanics, including stress–strain relationships, deformation, and failure theories. The software employs various constitutive models, such as elasticity, elastoplasticity, and caprock models, to represent the complex behavior of geological materials under different loading conditions. These models are essential for understanding how reservoir rocks react to the injection of CO<sub>2</sub>, including potential fracturing and changes in permeability and porosity.

The CMG-GEM geomechanics module leverages three fundamental equations to simulate the mechanical response of rock formations to CO<sub>2</sub> injection. The equilibrium Equation (7) asserts the force balance within the reservoir, indicating that the divergence of the stress tensor ( $\sigma$ ) is balanced by body forces ( $B$ ). The strain–displacement Equation (8) relates the deformation of the reservoir to displacement fields ( $u$ ), which is essential for understanding how the rock fabric responds to changes. Finally, the stress–strain Equation (9) ties the strain ( $\epsilon$ ) within the rock to the induced stress, incorporating the impact of pore pressure ( $p$ ), temperature change ( $\Delta T$ ), and rock stiffness, embodied in the stiffness tensor ( $K$ ) [63]. These core relationships are integral to predicting the deformation of the rock, its fracturing potential, and changes in permeability and porosity, all critical for assessing the effects of CO<sub>2</sub> injection.

$$\nabla \cdot \sigma - B = 0 \quad (4)$$

$$\epsilon = \frac{1}{2} (\nabla u + (\nabla u)^T) \quad (5)$$

$$\sigma = K : \epsilon + (\alpha p + \eta \Delta T) I \quad (6)$$

where

$\sigma$  represents the stress tensor;  
 $B$  denotes body forces;  
 $\epsilon$  is the strain tensor;  
 $u$  is the displacement vector;  
 $K$  is the stiffness tensor;  
 $\alpha$  is the Biot coefficient;  
 $p$  stands for pore pressure;  
 $\eta$  is the thermoelastic coefficient;  
 $\Delta T$  represents the temperature change;  
 $I$  is the identity tensor.

In this study, linear elastic modeling was adopted in our flow-geomechanics simulations of ground deformation due to CO<sub>2</sub> injection. This conservative approach aligns with our focus on understanding ground deformation. It is worth noting that if plasticity were to occur, it would likely lead to even larger displacements. Therefore, by using linear elasticity, we are taking a cautious approach and providing a baseline for potential deformation. This method strikes a balance between accuracy and computational efficiency, enabling us to realistically represent the mechanical behavior of the reservoir under CO<sub>2</sub> injection stress while managing computational resources effectively.

Our reservoir model's predictive capability for geomechanical responses to CO<sub>2</sub> injection is contingent on an accurate representation of the in situ stress profile. This profile is established by mapping pore pressure and minimum total stress from a depth of



–2900 m to –3400 m within the injection well. These mappings are important for evaluating rock deformation potential and failure risk. We assume hydrostatic conditions for the pore pressure gradient, while the minimum stress gradient is aligned with observed values for passive margin regimes, specifically reflecting the low tectonic stress environment of Bra'il's offshore Campos Basin. By applying a stress gradient of roughly 22 kPa/m, our model captures the geomechanical nuances of the Campos Ba'in's passive margin stress regime [75–77].

With respect to meshing, it was possible to employ a dual-grid system, which optimizes computational efficiency. Figure 4 shows the grid of the model used in this work, with 421,344 elements. In this study, we maintain a consistent grid for both fluid flow and geomechanical simulations across the entire model. This approach offers a significant difference from typical reservoir geomechanics studies, where flow is often simulated only within the reservoir, while geomechanical calculations are extended to the surrounding formations. By applying this approach, the essential processes, such as the dissipation of pressure beyond the confines of the reservoir, can be captured. This method ensures that no critical physical interactions are overlooked, addressing a gap that is often present in geomechanical studies [4,42,78,79].

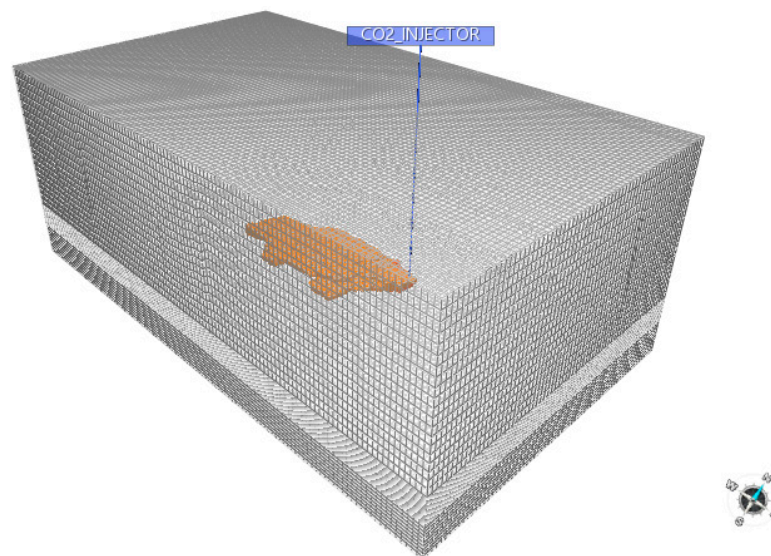


**Figure 4.** UNISIM-I extended model grid for flow and geomechanical simulations.

This study considers a one-way coupling option for integrating the reservoir simulator with the geomechanical module. The one-way coupling allows for representing the impact of fluid flow on geomechanics without considering the reverse effect. This approach is suitable for studies where the influence of geomechanical changes on fluid dynamics is not a primary concern. On the other hand, the full coupling method allows for a more interactive exchange between fluid flow and geomechanics, with either solving each aspect in turn and updating their states iteratively [80] or applying a monolithic approach [81]. A fully coupled method is more suited for analyses requiring a nuanced understanding of fluid dynamics and rock mechanics [82].

While the software offers multiple ways to couple these simulations, ranging from fully coupled to one-way interactions, for our specific study, we have chosen to use a one-way coupling approach. This decision aligns with our study's objective, as we are not investigating the feedback of geomechanical responses on fluid dynamics. The chosen method balances computational efficiency and the accuracy needed for our analysis, allowing us to dynamically simulate the reservoir's behavior concerning CO<sub>2</sub> injection without the added complexity of full coupling.

## 5. Methodology and Results

The methodology employed in this study characterizes the diffusion of pressure in porous media resulting from CO<sub>2</sub> injection and its impact on the ground deformation during and after the cessation of the injection. This analysis has been carried out using the UNISIM-I model described in the previous sections, which features a large, single-shale caprock. By utilizing this model, we explore the geomechanical impacts of CO<sub>2</sub> injection, specifically simulating ground uplift, the interplay between rock properties, injection rates, pressure buildup, and CO<sub>2</sub> migration. Additionally, we investigate the role of caprock in pressure dissipation, offering insights into optimizing monitoring strategies. Furthermore, a sensitivity analysis is conducted to broaden the scope of our conclusions by considering various levels of mechanical rock properties and different rates of CO<sub>2</sub> injection.

### 5.1. CO<sub>2</sub> Injection Flow Results

In the simulation, the CO<sub>2</sub> was injected at a constant rate of 2200 tons per day over 20 years, followed by 50 years of monitoring, resulting in 70 years of simulation. This extended duration was chosen to simulate realistic long-term injection scenarios, reflecting the commitment to sustained carbon sequestration efforts. The total injected volume culminated in 16 million metric tons of CO<sub>2</sub>, as depicted by the cumulative injection curve (Figure 5, blue curve) and the average reservoir pressure, showcasing an initial increase followed by a dissipation phase (Figure 5, red curve).

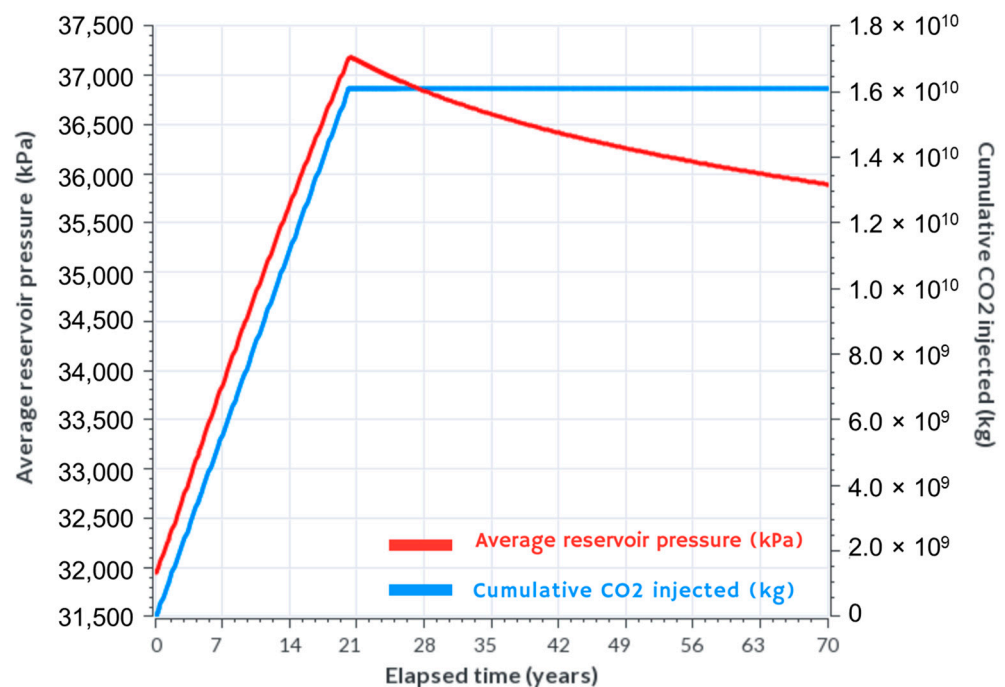


**Figure 5.** Reservoir pressure and cumulative CO<sub>2</sub> injection over 20 years and subsequent 50 years of monitoring period. The blue curve indicates the total CO<sub>2</sub> injected, while the red curve shows the corresponding average pressure in the reservoir.

The pressure increase during the injection period (Figure 5) can be interpreted as a clear response of the reservoir to the substantial volume of CO<sub>2</sub> being stored. The steep rise in pressure suggests that the aquifer has a limited capacity to accommodate the injected CO<sub>2</sub> without significant pressure buildup, which implies that the reservoir volume or the permeability may not be as large as required for the injected volumes. After reaching a peak, 20 years after the start of the injection, the pressure curve shows a gradual decline, signaling the onset of pressure dissipation. This phase transition may denote the beginning of CO<sub>2</sub> redistribution within the reservoir and potential migration into adjacent rocks, suggesting that the initial storage volume is approaching its capacity limit. The phase of

pressure decline may also suggest that the pressure is being alleviated not just within the reservoir but also across the surrounding rock formations.

This diffusion into the adjacent rocks can occur even in the absence of significant CO<sub>2</sub> migration due to the nature of pressure transmission through the pore fluids, which precedes the physical movement of CO<sub>2</sub>. The pressure within a fluid-filled porous medium can propagate more rapidly than the CO<sub>2</sub> itself due to the fluid's compressibility and the interconnectedness of the pore spaces, allowing for a swift response and redistribution of pressure throughout the surrounding rocks.

Figure 6 captures the evolution of reservoir pressure via delta pressure visualizations, marking changes from the initial state due to CO<sub>2</sub> injection. Figure 6A is the 3D view at the end of the 20-year injection phase, and it shows a relevant delta pressure gradient not only around the injector, with warmer hues indicating more significant pressure increases, but also within the entire confined reservoir. This confinement and the magnitude of pressure buildup at the injection end, evident from the vibrant coloration in Figure 6A, present subsequent long-term dissipation into the surrounding shaly rocks. Figure 6B's vertical cross-section near the injector after 20 years reveals the onset of this dissipation, with color transitions highlighting pressure migration beyond the reservoir boundaries.

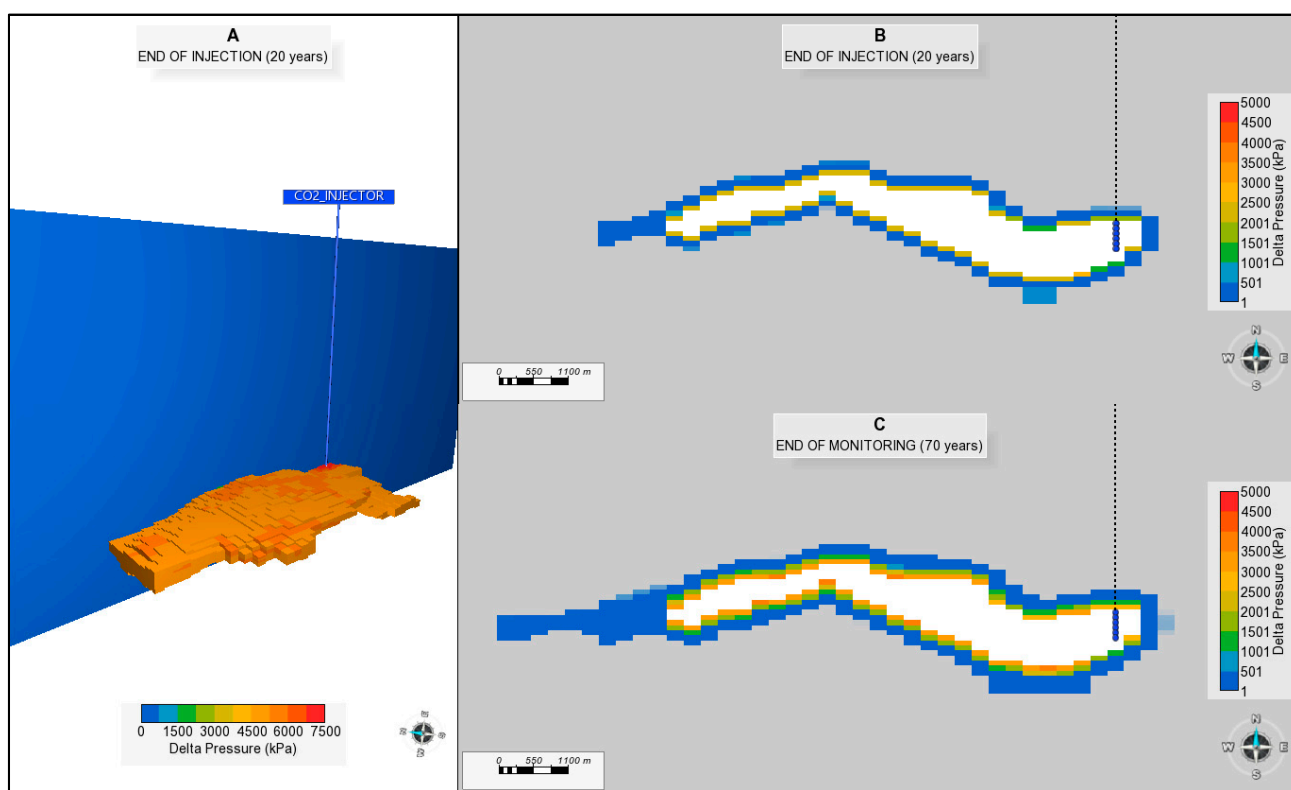


**Figure 6.** Delta pressure (difference between initial and current pressure per gridblock) distribution in the reservoir and surrounding rocks. Panel (A) shows a 3D view of the reservoir at the end of the 20-year CO<sub>2</sub> injection phase, indicating high delta pressure near the injection well. Panels (B,C) depict vertical cross-sections at 20 and 70 years, respectively, highlighting pressure dissipation into the surrounding shaly rocks over time. On panels (A,B), the reservoir is depicted in white.

By 70 years, Figure 6C illustrates that the pressure has dissipated even further into the surrounding rocks. This extended spread of pressure, despite the absence of considerable CO<sub>2</sub> movement (Figure 7), indicates that the diffusion of pressure through the fluid phase outpaces the physical redistribution of CO<sub>2</sub>, emphasizing the role of the interconnected pore network in the broader geological environment for managing injected pressures. The visual data from Figure 6B,C corroborate the effects of the injection on the adjacent rocks,

which accommodate and redistribute the excess pressure over the long term, as observed by other authors in similar analyses regarding the caprock's integrity [83,84].

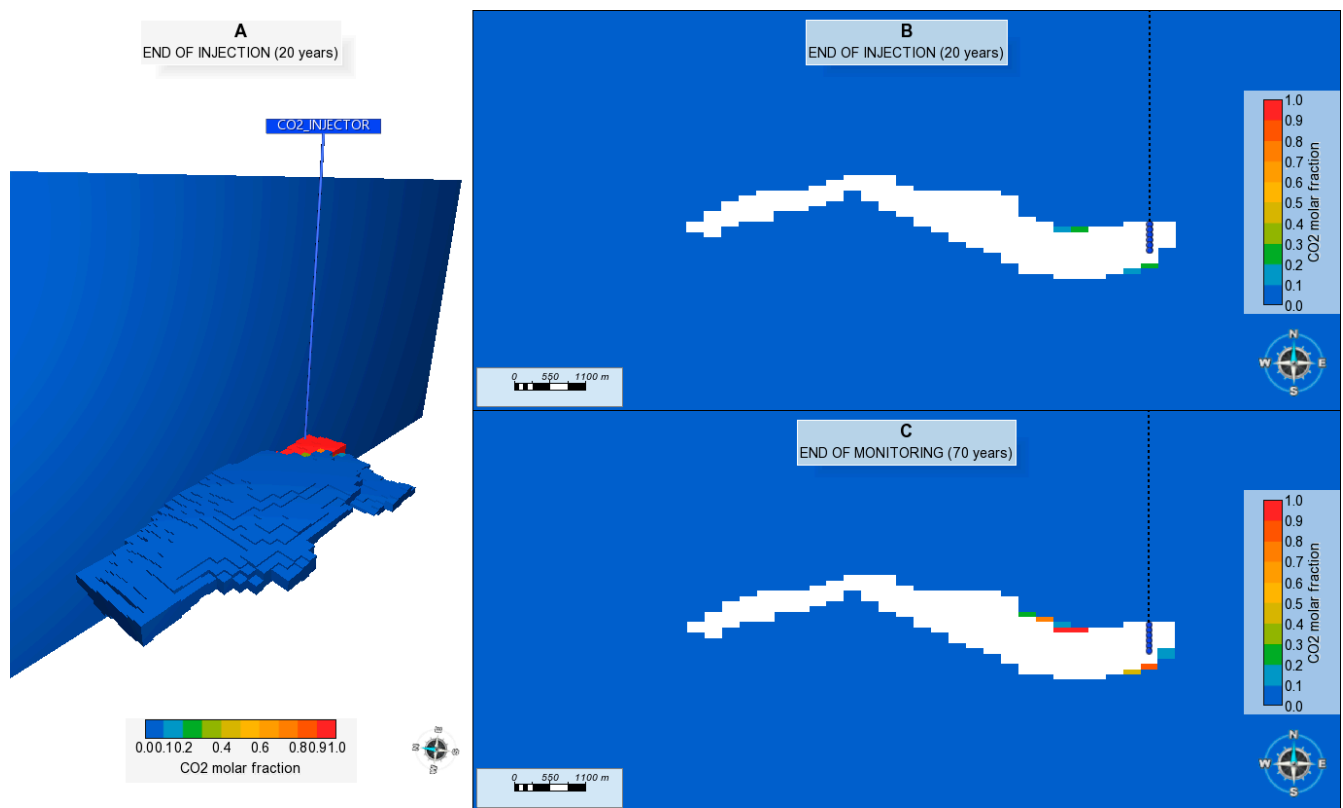


**Figure 7.** CO<sub>2</sub> global molar fraction post-injection and monitoring phases. Panel (A) shows the CO<sub>2</sub> concentration around the injector at the end of the 20-year injection period. Panels (B,C) reveal vertical cross-sections at 20 and 70 years, respectively, with minimal CO<sub>2</sub> migration into the caprock. On panels (A,B), the reservoir is depicted in white.

In Figure 7, the distribution of the CO<sub>2</sub> molar fraction within the reservoir and its immediate vicinity is illustrated at two distinct time points: at the end of the injection period and after an extended monitoring phase. Figure 7A shows a 3D view at the 20-year mark, with the CO<sub>2</sub> molar fraction concentrated around the injector, where red denotes the highest concentration. The presence of CO<sub>2</sub> within the reservoir is contained primarily due to the significant capillary pressure in the shale caprock and its low permeability, which act as barriers to migration. Figure 7B,C depict vertical cross-sections near the injector well at 20 and 70 years, respectively. At the end of the injection phase (Figure 7B), the CO<sub>2</sub> has predominantly remained within the reservoir boundaries. By 70 years (Figure 7C), there is a slight presence of CO<sub>2</sub> detectable in the surrounding rock formation mainly through diffusion or a numerical artifact driven by diffusion due to the coarse grid considered in our model, as discussed in [59,85]. However, this penetration is minimal and does not constitute a leakage concern as absence of fractures or other flow localization features in this model is assumed. The limited movement of CO<sub>2</sub> into the surrounding rocks illustrates the combined influence of the caprock's low permeability and the high capillary entry pressure, which together serve as a robust containment mechanism, ensuring the long-term integrity of the geological storage.

Understanding the behavior of the CO<sub>2</sub> plume within the geological storage is important for assessing the effectiveness of carbon capture and sequestration strategies. Observing the plume's behavior over time allows us to confirm that the physical characteristics of the reservoir and the injected CO<sub>2</sub> are in agreement with predictive models, ensuring the reliability of long-term storage solutions. In this context, Figure 8 illustrates the CO<sub>2</sub>

migration within the reservoir at two times. The left panel of Figure 8 reveals the state of the reservoir immediately after 20 years of injection, highlighting the buoyant rise of CO<sub>2</sub> towards the less dense upper regions, a behavior that underscores the consistency of our simulation's fluid and rock physics. The right panel demonstrates the situation after 70 years. In this period between 20 and 70 years, the CO<sub>2</sub> within the reservoir has moved upward but not significantly beyond its boundaries, indicating the effectiveness of the caprock's structural integrity and capillary forces in limiting vertical movement. This containment is further evidenced by the minimal lateral dispersion into the surrounding rocks, evidencing the robustness of natural trapping mechanisms and the security of CO<sub>2</sub> storage over an extensive monitoring period.

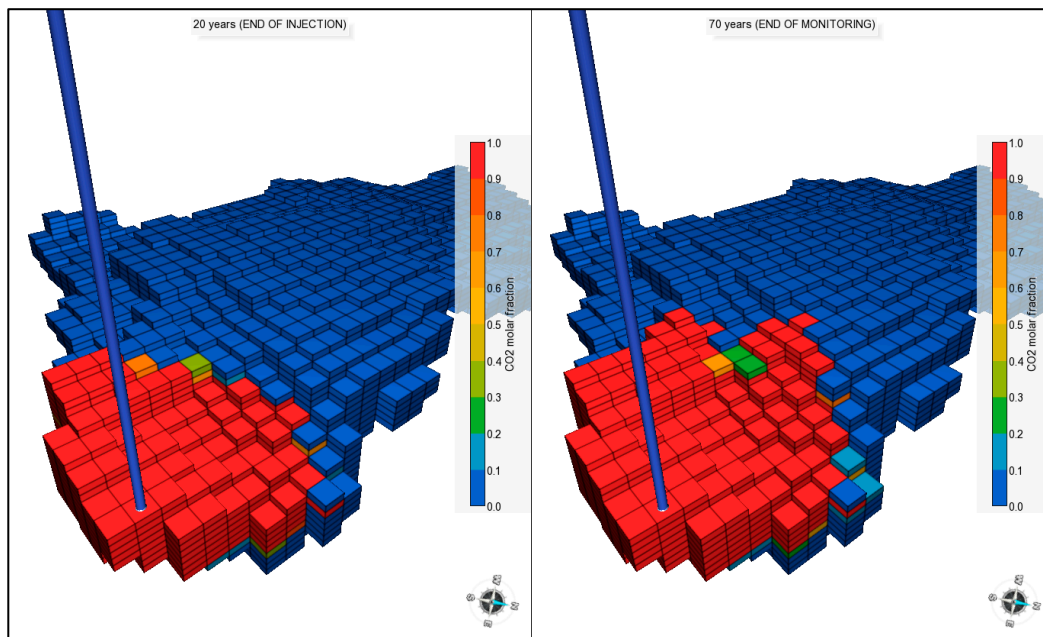


**Figure 8.** CO<sub>2</sub> global molar fraction distribution at the end of injection and post-monitoring periods. The (left) illustrates the reservoir immediately after the 20-year injection phase and the (right) panel reveals the CO<sub>2</sub> distribution after 70 years.

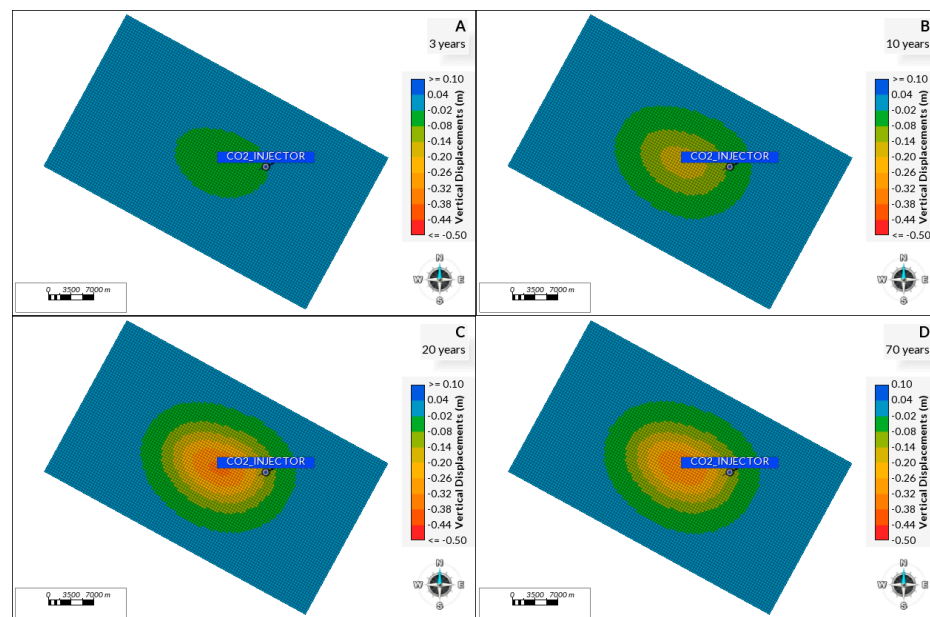
Even using a coarse mesh, the model was able to capture the vertical movement of CO<sub>2</sub>, demonstrating the buoyant rise and containment within the geological formation over time. This outcome suggests that even with less detailed spatial resolution, key processes governing CO<sub>2</sub> migration and trapping can be effectively simulated, providing valuable insights into the overall behavior of the CO<sub>2</sub> plume. However, if the primary objective of a study is to investigate the nuanced details of CO<sub>2</sub> plume dynamics, such as precise migration paths or small-scale heterogeneities within the reservoir, a much finer grid should be considered. A refined mesh would enhance the model's ability to capture fine-scale physical processes and interactions, offering a more detailed and accurate representation of CO<sub>2</sub> behavior within the subsurface. This is especially important for projects where the exact delineation of the CO<sub>2</sub> plume and its interaction with the geological environment are critical.

## 5.2. Geomechanical Results

Following an examination of the pressure impacts from CO<sub>2</sub> injection and the resultant CO<sub>2</sub> distribution within the reservoir, we now analyze the geomechanical responses. This part of the study addresses questions raised earlier, such as the practicality of using uplift measurements for monitoring purposes and the implications of subsidence patterns over the long term. We also look at how these ground movements relate to the position of the injection well and the dissipation of pressure during the post-injection phase. Additionally,

strategies for the strategic placement of monitors are considered, aiming to enhance the detection of vertical deformations.

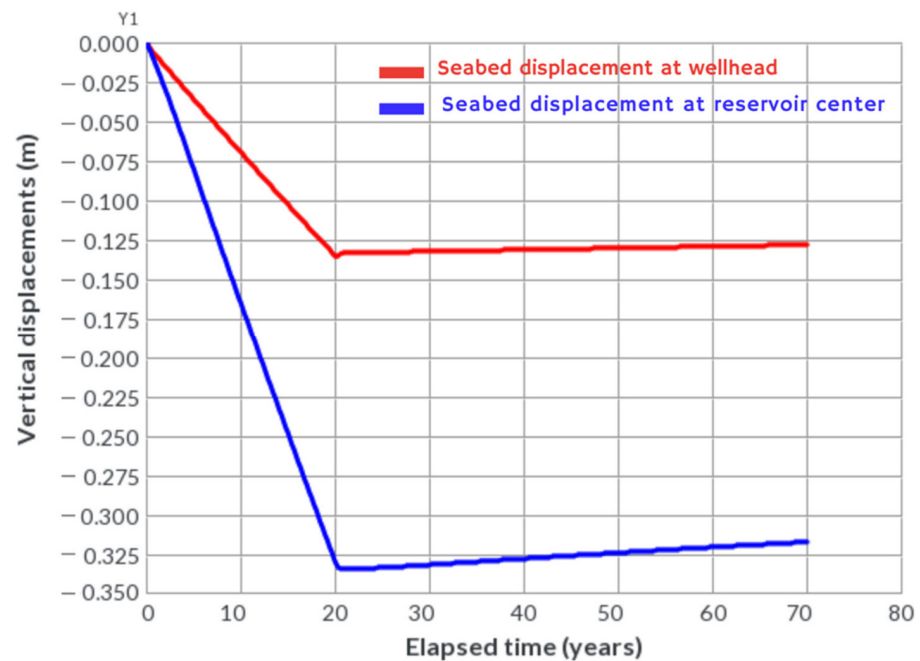
Figure 9 illustrates the temporal evolution of seabed uplift due to subsurface CO<sub>2</sub> injection, captured at four different times: 3, 10, 20, and 70 years. The negative values shown correspond to an upward displacement against the downward-oriented Z-axis, reflecting rock expansion as a result of CO<sub>2</sub> injection. Initially, significant uplift is observed, especially around the 20-year mark, indicating significant rock expansion due to CO<sub>2</sub> injection and the reservoir pressure buildup. Over time, as the injection ceases and the system begins to equilibrate, the 70-year mark reveals a slightly decreased uplift at the reservoir's center. This change is attributed to the dissipation of pressure into the surrounding rock formations, which acts as a pressure-relief mechanism for the reservoir.



**Figure 9.** Seabed uplift progression over time due to CO<sub>2</sub> injection. Panels (A–D) show the seabed uplift at 3, 10, 20, and 70 years, respectively. The uplift is depicted as negative values of subsidence, signifying upward movement.

The uplift is not uniform, with the largest displacement occurring slightly away from the wellhead, indicative of the CO<sub>2</sub> migrating towards the flank of the reservoir where the structural conditions are conducive to upward movement. This suggests a more pronounced rock expansion in these shallower areas of the reservoir, with less overburden stress facilitating uplift. These insights challenge conventional expectations, particularly the intuitive anticipation of the largest displacements occurring at the wellhead location [36]. They emphasize the importance of a detailed understanding of temporal geomechanical changes for the design and monitoring of CO<sub>2</sub> sequestration sites, highlighting the need for a comprehensive approach to address the implications of these changes on long-term storage integrity.

The graph in Figure 10, showcasing vertical displacement at the wellhead (red) and the center of the reservoir (blue), provides a key insight into the geomechanical changes during and after CO<sub>2</sub> storage. This phenomenon implies that the subsurface system is still dynamically adjusting to the introduced CO<sub>2</sub> long after the injection phase has concluded. The data reveal a persistent ground movement due to pressure dissipation, extending beyond the injection period, which represents significant insight into the behavior of the storage system. It shows that the ground deformation rate is not null after the end of injection and that it can still be used as a source of data to be captured. Thus, their deployment can provide continuous monitoring of the geomechanical state of the CO<sub>2</sub> storage site.



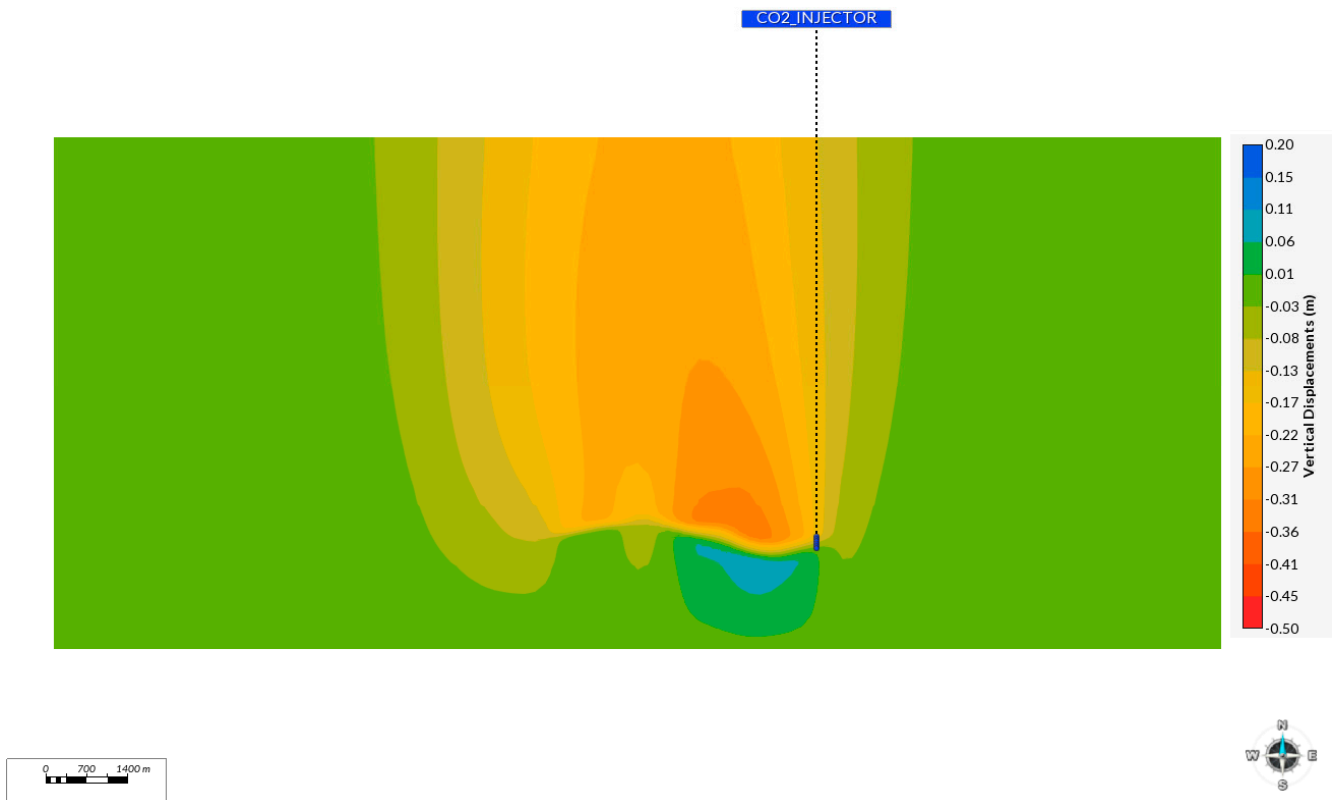
**Figure 10.** Seabed vertical displacement at wellhead (red) and reservoir center (blue) over time. Negative values indicate upward movement.

Figure 11 illustrates the geomechanical behavior at the end of the 20-year injection period and brings a key insight related to the unexpected location of maximum uplift, which, as depicted in the vertical cross-section of the model, is not at the wellhead but rather closer to the center of the reservoir. This area, being shallower, is subject to less overburden stress, making it more responsive to the pressure changes induced by the injection process. The significance of this finding extends beyond mere observation; it underscores the critical need for precise geomechanical modeling before the implementation of monitoring strategies. While the highest delta pressure remains near the injection point, the most substantial uplift occurs in a different location, influenced by the reservoir's structural nuances. This highlights the heterogeneous nature of the reservoir's response to CO<sub>2</sub>.

Insights like these help with accurately determining the optimal placement of monitoring instruments, such as tiltmeters, within the so-called Area of Review, as described in the Introduction.

To illustrate the dynamic nature of ground displacement associated with CO<sub>2</sub> injection, Figure 12 shows the displacement rate (millimeters per year) at various times. It is particularly noteworthy that the highest displacement rate undergoes a significant shift in a relatively short period. Initially, the greatest displacement rate is observed in the vicinity of the CO<sub>2</sub> injector. However, as time progresses, this zone of maximum displacement migrates away from the injector, reaching a point further from the wellhead and above the center of the reservoir in a period of 3 months. This pattern is evident as early as 3 months into the injection process and becomes more pronounced at the 3-year mark.

At the injection shutoff, 20 years, the displacement is substantially pronounced, while by the 21st year, there is a significant reduction in displacement velocity, indicating the beginning of stabilization. It is important to point out that after CO<sub>2</sub> injection is stopped (after 20 years), the ground movement near the wellhead drops below 1 mm/year, which might be too small for some sensors to detect. Such observations are critical for understanding the temporal and spatial evolution of deformation, thereby aiding in the optimal placement of monitoring equipment.



**Figure 11.** Vertical cross-section showing reservoir deformation at 20 years. The color gradient represents the magnitude of uplift, with the CO<sub>2</sub> injector indicated by the dashed line and the point of maximum uplift highlighted in the central region, offset from the injector.

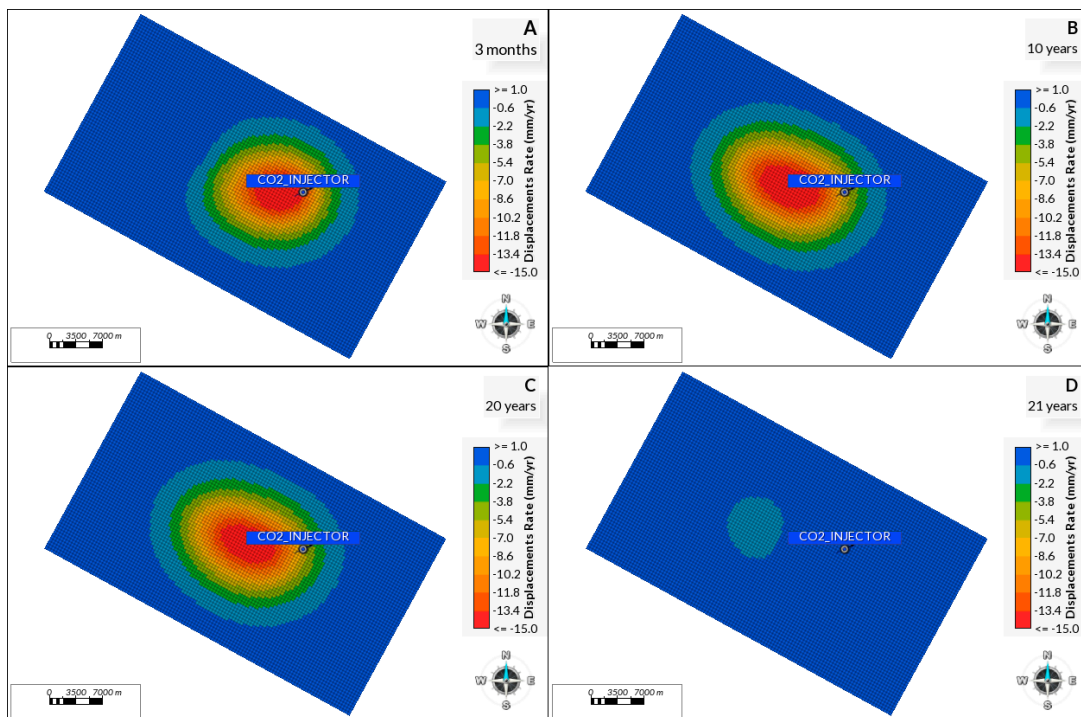


**Figure 12.** Vertical displacement rates in mm/year at intervals following CO<sub>2</sub> injection start. Panels (A–D) show the seabed vertical displacement rates at 3 months, 20 years, and 21 years, respectively.



As we conclude this section, we have laid a robust foundation for a simulation framework that not only highlights the critical insights gained from monitoring ground deformation and pressure dissipation but that also underscores the intricacies of CO<sub>2</sub> redistribution within the geological storage. These insights are paramount for the development of effective and secure Carbon Capture and Storage strategies and to further refine our understanding of geomechanical responses to CO<sub>2</sub> storage. Moving forward, this study will embark on a series of sensitivity analyses. This next phase is designed to evaluate how variations in key parameters—such as the mechanical properties of rocks, caprock permeability, and CO<sub>2</sub> injection rates—impact our findings. The sensitivity analyses aim to further refine our understanding of geomechanical responses to CO<sub>2</sub> storage, ensuring that the conclusions drawn are robust and applicable across a range of scenarios. This will enhance the predictive accuracy of our models, contributing to the optimization of CO<sub>2</sub> sequestration practices and the advancement of monitoring technologies.

### 5.3. Sensitivity Analysis

The forthcoming phase of this study will center on a sensitivity analysis to elucidate the effects of variations in rock mechanical properties, caprock permeability, and CO<sub>2</sub> injection rates on the geomechanical behavior associated with GCS. Detailed ranges of the parameters under consideration for the uniform distribution of properties are delineated in Table 4, and the designated points of interest within the 3D geomechanical model are highlighted in Figure 13.

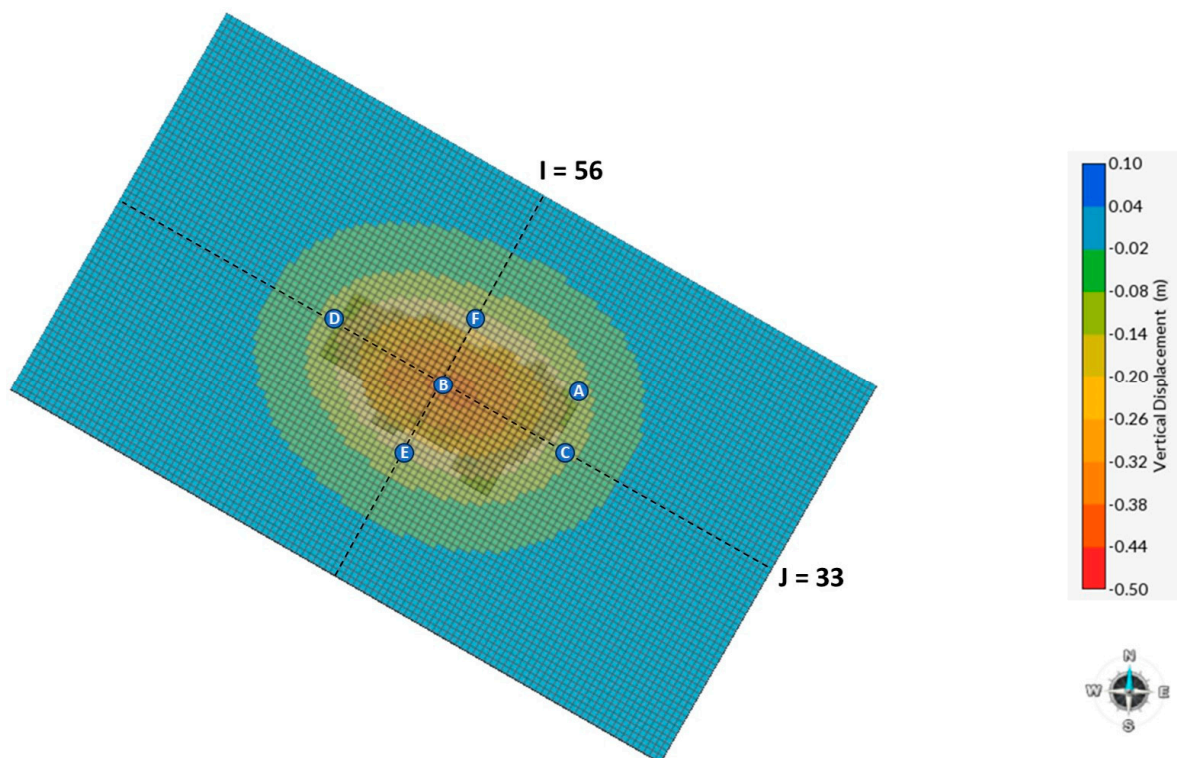


**Figure 13.** Monitoring points of interest for geomechanical sensitivity analysis. The figure displays points A–F, indicating areas of interest against a backdrop depicting vertical displacement. Points A and B represent the wellhead and the central reservoir peak displacements in m, respectively. The orthogonal I and J grid paths intersect at the reservoir’s surface midpoint, situating these points within the model.

**Table 4.** Ranges of the uniform distribution of the parameters used in the sensitivity analysis [55,56].

Property	Min Value	Max Value
Injection rate (tons/day)	100	3000
Poisson's ratio (sandstone)	0.22	0.39
Poisson's ratio (shale)	0.28	0.48
Young's modulus (sandstone) (GPa)	0.7	34
Young's modulus (shale) (GPa)	6.9	69
Caprock permeability (mD)	$10^{-9}$	$10^{-2}$

Upon defining the range of parameters for this study, 80 realizations were executed to produce an ensemble of displacement curves, as visualized in Figure 14. Panel A corresponds to the path along  $J = 33$ , while Panel B represents  $I = 56$ . These figures are crucial, as they demonstrate a significant dispersion in the displacement outcomes, indicative of the varied responses within the model to changes in  $\text{CO}_2$  injection rates. The maximum vertical displacement reaches approximately  $-0.35$  m, while some models barely have it. It is important to note that these displacements occur after the  $\text{CO}_2$  injection after 20 years, representing the expected maximum displacement within the modeled timeframe. The spread of the displacement curves underscores the importance of considering a wide range of scenarios to adequately capture the complexities and uncertainties inherent in geomechanical behavior during  $\text{CO}_2$  storage operations.

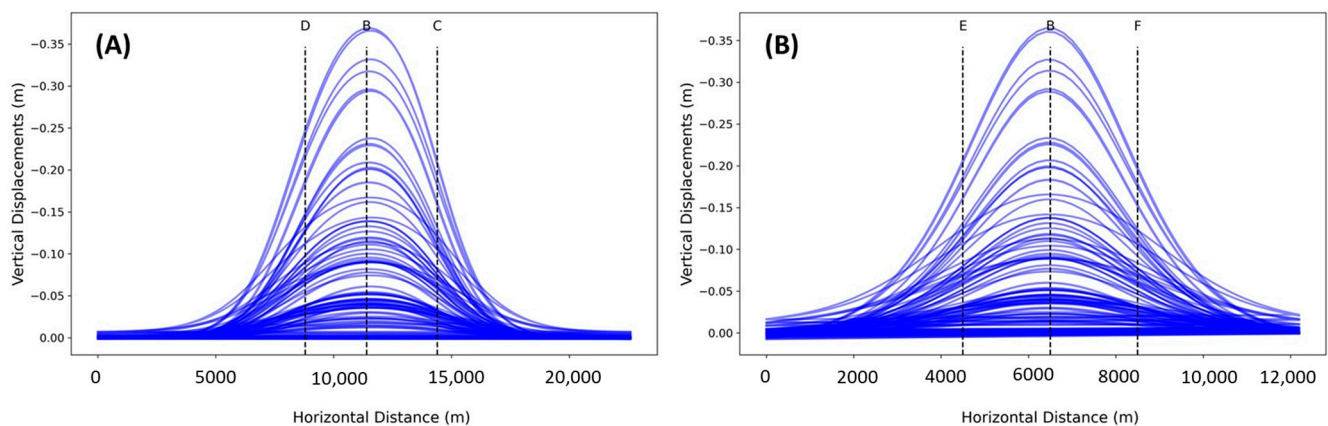


**Figure 14.** Ensemble of vertical displacement curves post-injection. Panel (A) ( $J = 33$ ) and Panel (B) ( $I = 56$ ) display the range of vertical displacements resulting from 80 realizations based on varied parameter inputs.

In Figure 15, vertical displacements along path  $J = 33$  are analyzed and depicted, with displacement curves distinctly color-coded to represent a spectrum of sensitivity parameters utilized in this study. The visual data suggest that rocks with higher Poisson ratios and lower Young's modulus values—attributes that contribute to a rock's ductility and stiffness—experience increased vertical displacements. Additionally, increased  $\text{CO}_2$  injection rates and reduced shale permeabilities are associated with greater displacement magnitudes. Such trends are indicative of the complex interplay between rock mechanics and the operational parameters of  $\text{CO}_2$  injection, underscoring the need for meticulous evaluation in the design and monitoring of  $\text{CO}_2$  sequestration initiatives, because not considering the uncertainty in rock properties could lead to significant errors in vertical displacement predictions.

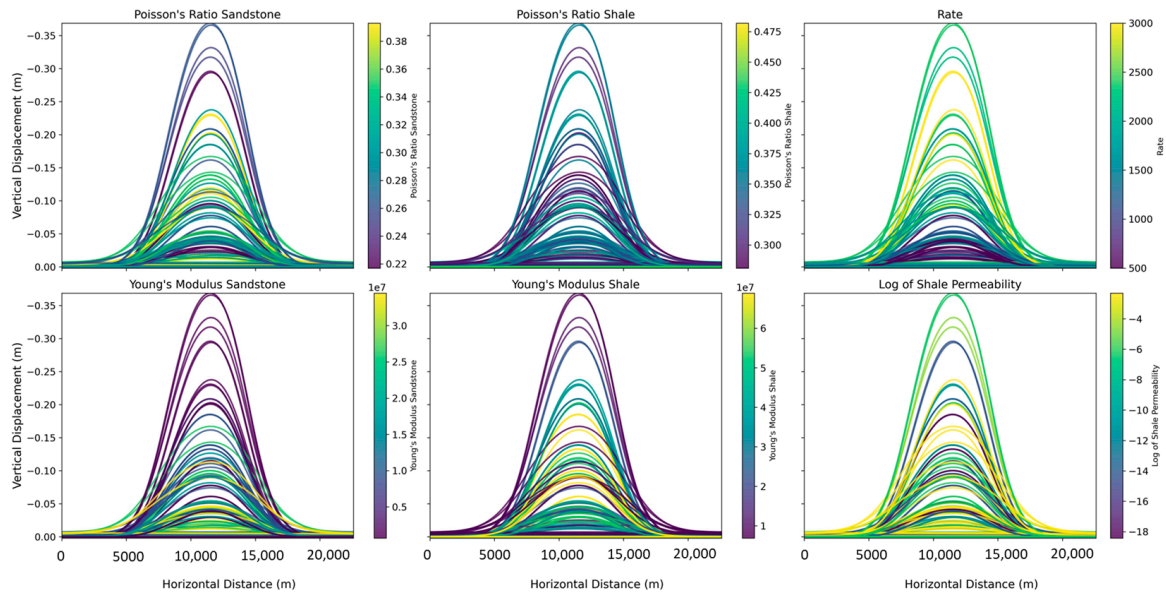


**Figure 15.** Sensitivity analysis of vertical displacement curves along path J = 33. Displacement curves are stratified by parameters used in the sensitivity analyses.

The statistical analysis aimed at understanding the variability and range of geomechanical responses at various monitoring points is presented in Figure 16, parts A and B. The box plots in part A of the figure synthesize the central tendencies and dispersions of vertical displacements observed at each monitoring point (A–F) after 20 years of CO<sub>2</sub> injection. They illustrate a distinct pattern. Monitoring point B, situated at the reservoir’s projected center, consistently experiences the largest vertical displacements. This pattern is indicative of the pressure distribution and stress diffusion within the reservoir, highlighting the central region as the primary locus of geomechanical impact due to CO<sub>2</sub> injection. Part B of Figure 16 assesses the impact of geomechanical properties on these vertical displacements, demonstrating that the mechanical properties, as characterized by Young’s modulus for both sandstone and shale, have effects on displacement comparable to those of the CO<sub>2</sub> injection rate. This emphasizes the significance of obtaining precise geomechanical properties to effectively characterize the rock and its caprock in GCS projects.

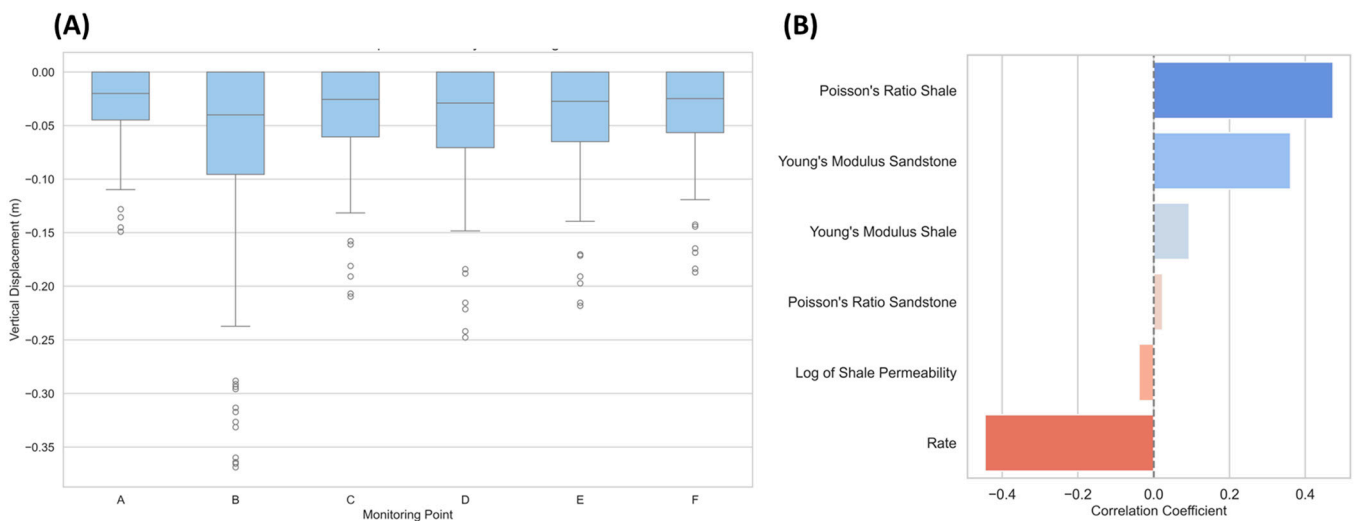


**Figure 16.** Integrated analysis of geomechanical responses’ and properties’ impacts on vertical displacement. Panel (A) presents box plots of vertical displacements at monitoring points A–F. Panel (B) quantifies the correlation between geomechanical properties and vertical displacement.

The negative correlation coefficients signify that an increase in these mechanical properties correlates with more significant upward displacement, emphasizing that the mechanical constitution of the reservoir plays a critical role in the deformation observed, alongside the operational parameters of the injection. This parallel in impact underscores the dual importance of understanding both the inherent mechanical behavior of the geological formation and the operational dynamics of CO<sub>2</sub> injection in managing geomechanical risks in GCS projects.

Figure 17 presents the correlations between geomechanical properties and vertical displacements at individual monitoring points within the reservoir after twenty years of CO<sub>2</sub> injection. Subplots A through F denote these points, indicating localized responses. The correlation coefficients, derived from variables including Young's modulus, Poisson's ratio for sandstone and shale, and CO<sub>2</sub> injection rates, reveal a multifaceted relationship that aligns with the overall behavior patterns identified across the reservoir. This suggests that the geomechanical behavior at single monitoring points reflects the broader, systematic influences of the injection process.

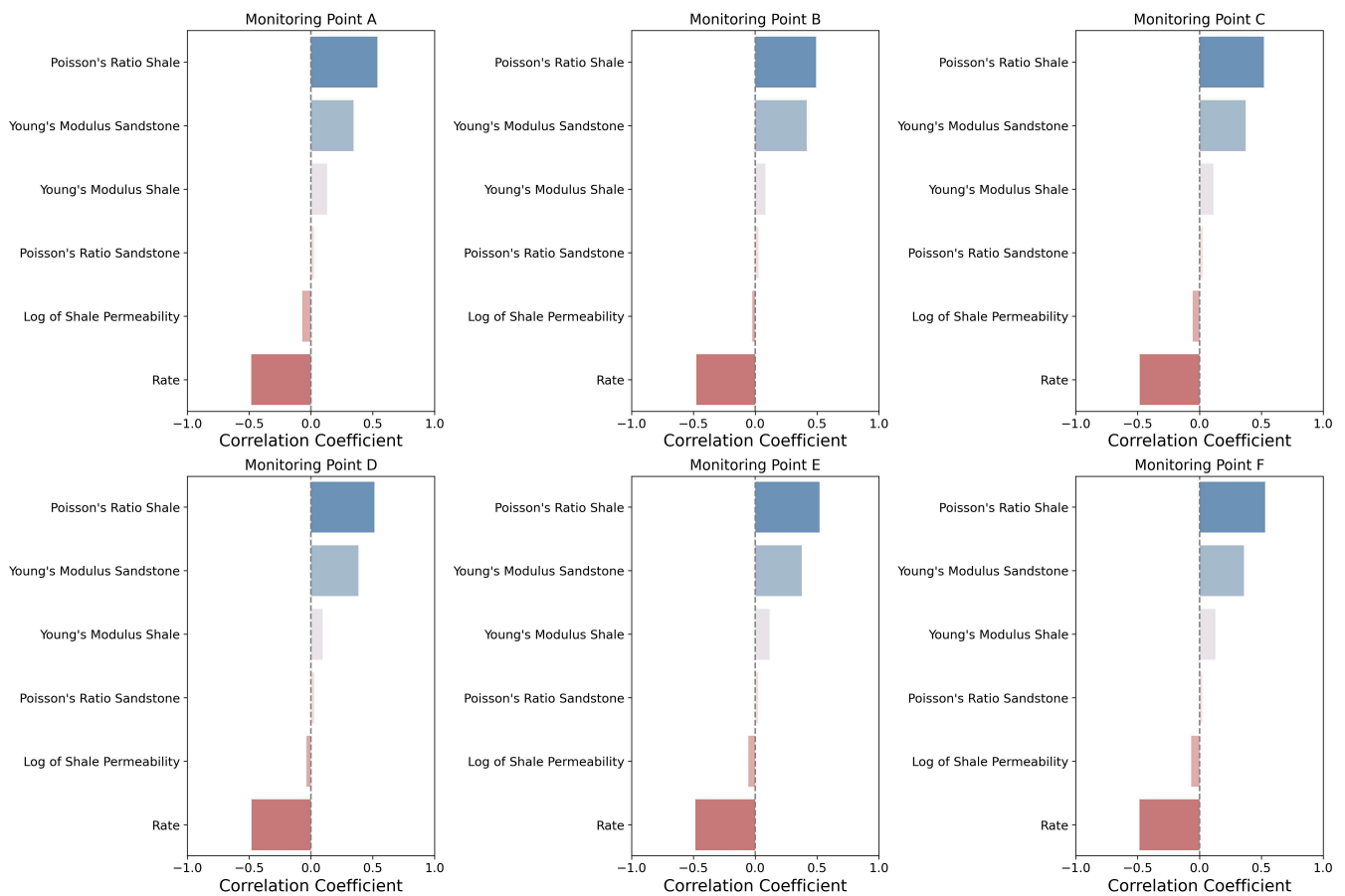


**Figure 17.** Correlation coefficients by monitoring point for geomechanical properties impacting vertical displacement. This figure demonstrates the correlation between geomechanical properties and vertical displacement, disaggregated by monitoring points (A–F).

Building on the comprehensive analyses detailed earlier, this study progresses to evaluate the influence of shale permeability on the dissipation of reservoir pressure over time in Figure 18. It depicts the interplay between shale permeability, CO<sub>2</sub> injection rates, and their combined effects on reservoir pressure over time. Panel A shows the influence of shale permeability on reservoir pressure, and it is observed that except for very low permeability scenarios ( $10^{-6}$  mD to  $10^{-9}$  mD), reservoir pressure decreases significantly after the cessation of CO<sub>2</sub> injection. This trend suggests that while shale

acts as a semi-permeable barrier, its permeability is crucial in regulating the rate at which pressure normalizes post-injection. For reservoir management, this implies that higher shale permeability can potentially be harnessed to mitigate risks associated with overpressure, provided that the permeability does not compromise the seal's integrity. Conversely, very low permeability could pose challenges in pressure management, possibly leading to an increased risk of induced seismicity or caprock failure.

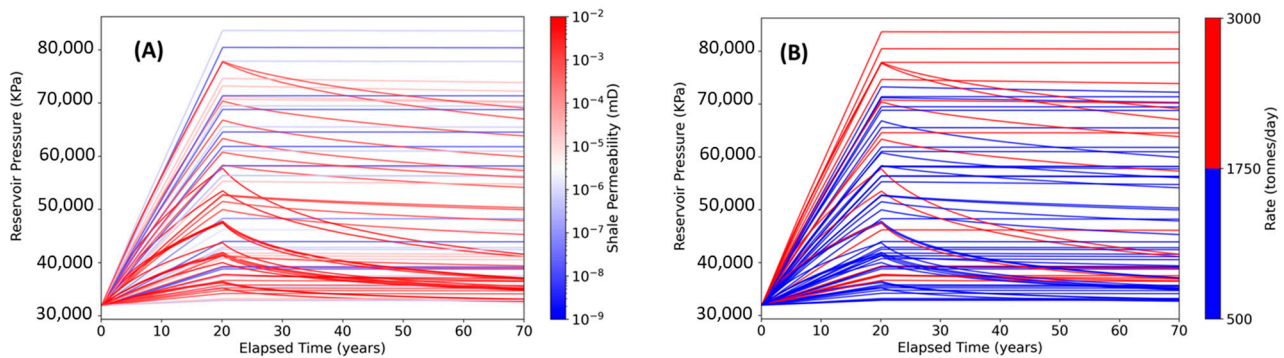


**Figure 18.** Panel (A) displays the effect of shale permeability on reservoir pressure after CO<sub>2</sub> injection. Panel (B) shows the impact of varying CO<sub>2</sub> injection rates on reservoir pressure across different caprock permeabilities.

Panel B further elaborates on the effect of injection rates on reservoir pressure. It demonstrates that under typical conditions [86,87], increased injection rates are associated with a proportional rise in average reservoir pressure. However, when juxtaposed with high caprock permeability, the anticipated linear relationship between injection rates and pressure is disrupted. This suggests that at higher permeabilities, the caprock may allow for a more rapid dissipation of pressure, thereby muting the impact of increased injection rates on overall reservoir pressure. From a practical standpoint, Panel B suggests that for effective CO<sub>2</sub> storage and containment, both the injection rate and the caprock permeability must be considered. Injection strategies should be tailored to balance the rate of CO<sub>2</sub> being injected with the permeability characteristics of the caprock to maintain desired pressure levels without compromising seal integrity or storage capacity.

Addressing the sensitivity in the vertical displacement rates is important because it is a threshold of detectability for several monitoring tools [41]. Figure 19 presents the vertical displacement rates at monitoring points A (wellhead) and B, with a focus on the detectability of such movements. The temporal scope of this figure spans 70 years, comprising both the active injection period and subsequent monitoring phases. A critical threshold delineates the detectable range of vertical displacements, demarcated as rates exceeding 1 mm/year in absolute value, with the shaded area representing the undetectable range (between  $-1$  and  $1$  mm/year). The vertical dashed line at 20 years marks the cessation of CO<sub>2</sub> injection, serving as a temporal delimiter for the analysis of displacement behaviors. At monitoring point B, the vertical displacement rates are predominantly higher than at monitoring point A (wellhead). Monitoring point B consistently demonstrates higher vertical displacement rates than point A (wellhead), reaffirming its suitability as a strategic location for enhanced detectability in geomechanical monitoring.

This analysis shows the advantage of optimizing the monitoring location, which, for the case study and parameters considered, would be monitoring point B, as it offers a higher probability of yielding detectable displacements across a broader spectrum of realizations. Post-injection, a decline in the vertical displacement rate is evident, with most realizations converging towards undetectable rates, falling within the  $\pm 1$  mm/year range. This reduction in rate suggests geomechanical stabilization within the storage formation, indicative of pressure redistribution and equilibrium attainment in the subsurface. However, some realizations still present detectable displacement rates for several years of monitoring point B. Interestingly, certain realizations reveal an inversion in displacement

trends, accentuating the reservoir's heterogeneity and the caprock's ability to assimilate and reallocate stress over time. This behavior is likely indicative of pressure diffusion effects within the caprock in specific scenarios. It is also probably an effect of the pressure diffusion on the caprock.

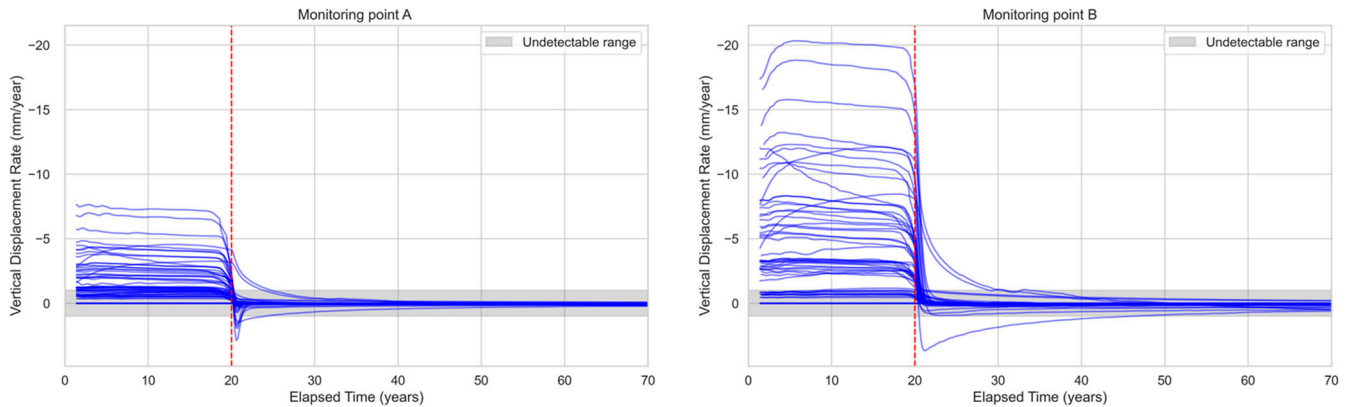


**Figure 19.** Vertical displacement rates at monitoring points (A) (wellhead) and (B). The undetectable range of vertical displacements is shaded, with a vertical dashed line indicating the end of CO<sub>2</sub> injection at 20 years.

Figure 20 presents the vertical displacement rates at monitoring points A and B, correlating the injection rates with the resulting vertical displacement rates. The expectation that higher injection rates would result in increased displacement is generally supported; however, the data do not show a simple one-to-one correspondence. The highest displacement rate is not associated with the peak injection rate, suggesting that displacement is influenced by a complex set of reservoir characteristics beyond just the injection rate. At monitoring point B, a range of injection rates, including some of the lower values, still result in displacement rates above the detection threshold. This demonstrates the sensitivity of this point and makes it a reliable location for monitoring detectable geomechanical changes among the other locations considered. In contrast, at point A, the wellhead, most displacement rates fall below the detection threshold, especially at lower injection rates, indicating less sensitivity to changes in CO<sub>2</sub> injection volume at this location.

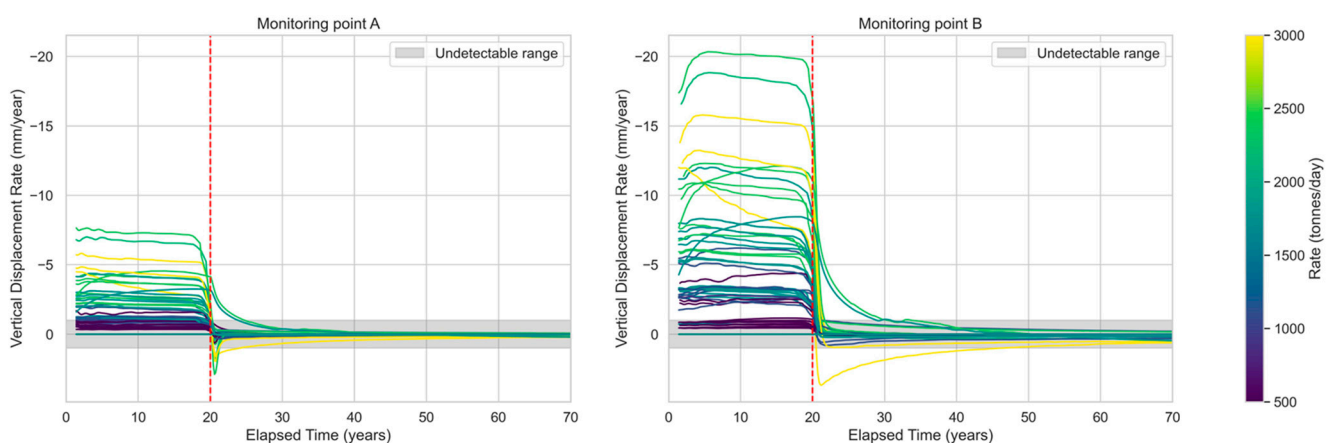


**Figure 20.** Vertical displacement rates at monitoring points (A,B) categorized by CO<sub>2</sub> injection rates, which are represented by a color gradient. The undetectable range of vertical displacements is shaded, with a vertical dashed line indicating the end of CO<sub>2</sub> injection at 20 years.

The sensitivity analysis provides insights into the geomechanical impacts of CO<sub>2</sub> storage operations. By examining a spectrum of parameters, this study has revealed

significant variability in geomechanical responses, which are important for enhancing the predictive accuracy of CO<sub>2</sub> sequestration models.

## 6. Discussion

The findings presented in this work underscore the need for comprehensive monitoring and robust calibration of models to effectively manage the geomechanical risks associated with CO<sub>2</sub> injection. The interdependencies between rock mechanical properties and operational parameters revealed through this analysis serve as a foundation for future research aimed at optimizing CO<sub>2</sub> storage strategies and ensuring the integrity of geological storage sites.

Expanding upon previous work on the positioning of a CO<sub>2</sub> injection well for GCS [57,58], our study discusses the impact of this placement of the well in a flank of the reservoir on the vertical displacements caused by the injection as a subsequent impact on the monitoring strategy. Adding to the discourse on geomechanical risks associated with GCS initiated by [15,18,19], our research emphasizes the importance of conducting sensitivity analyses on geomechanical modeling for the strategic selection of monitoring locations. This approach builds upon the insights from [21–24], who advocated for the need for accurate characterization of geomechanical properties and injection rates. Our study not only corroborates these findings but also advances the methodology by demonstrating how such analyses can optimize monitoring strategies, thereby enhancing the predictive accuracy and safety of GCS operations. Furthermore, we discuss the importance of explicitly modeling the flow within the caprock, a critical element often not addressed in coupled geomechanics studies that could help evaluate the true impact of geomechanics on the caprock. This underscores the impact of incorporating flow modeling in caprock analysis to ensure a comprehensive understanding of CO<sub>2</sub> storage safety and efficacy.

Moreover, our research sheds light on the critical interplay between injection rates, rock properties, and pressure buildup, a complex relationship that has been explored to a lesser extent in the literature. By providing a detailed analysis of how these factors influence CO<sub>2</sub> migration and ground deformation, our study offers a novel perspective that challenges the conventional selection of wellhead monitoring sites, as typically suggested by previous studies, like [40,41]. We reveal the limitations of traditional monitoring approaches in capturing the nuanced geomechanical responses to CO<sub>2</sub> injection, suggesting a reevaluation of monitoring strategies to better manage the associated risks.

It is important to consider the limitations of this study to ensure a nuanced understanding of our findings and to accurately direct future avenues of research. One consideration is the foundation of our analysis on simulations derived from a singular reservoir model. While providing valuable insights into the specific geological configuration examined, this approach may not encompass the diversity found in various geological settings where GCS is applicable. The results, while enlightening for the studied scenario, may not be broadly generalizable across all possible configurations of GCS. For reservoirs in which permeability is greatly affected by the changes in stress during injection, like naturally fractured rocks, the methodology could benefit from the integration of consistent coupling mechanisms. Additionally, the inclusion of chemical reactions in our modeling efforts could offer a deeper understanding of how these processes influence the geomechanical properties of subsurface formations, potentially unveiling new insights into the long-term stability and integrity of CO<sub>2</sub> storage sites.

Further investigation using fine-scale models is recommended to delve deeper into the mechanisms of enhanced CO<sub>2</sub> dissolution. The use of a finer grid in this model can provide a more detailed and accurate representation of the dissolution and other trapping processes. By conducting such investigations, a more comprehensive understanding of CO<sub>2</sub> entrapment in the caprock can be gained, thus enhancing the overall analysis and the findings of this study.

While our simulations provide valuable insights into GCS, the lack of field verification is a significant limitation. Theoretical models, no matter how detailed, need empirical data

to validate their predictions and enhance their credibility. Future efforts should focus on integrating field data from similar GCS projects into the theoretical models and compare their predictions with actual conditions. This integration would allow for the calibration of our model based on real-world outcomes, thus enhancing its predictive power and reliability. Although our model is based on simulations derived from a singular reservoir model, it offers a methodological framework that could be adapted for broader use. We recommend further investigation using field data from multiple geological settings to test the adaptability of our approach. Additionally, incorporating multi-scale data and chemical reactions into our models could deepen our understanding of subsurface dynamics, thus aiding in the design of more effective CO<sub>2</sub> storage solutions.

In addition to mechanical properties and CO<sub>2</sub> injection rates, our focus in this study, we recognize the potential influence of considering a broader range of parameters in the sensitivity analyses, such as permeability, porosity, relative permeabilities, and fluid properties, and their impacts on the outcomes of CO<sub>2</sub> injection scenarios. These parameters play important roles in the dynamics of GCS, but they were not extensively analyzed due to their vast variability and complex interaction effects. Including a comprehensive sensitivity analysis incorporating these hydrodynamic and fluid properties would have expanded the scope and increased the complexity of our study significantly. Therefore, while our focused approach provided essential insights into the geomechanical impacts of CO<sub>2</sub> injection, future studies could benefit from an expanded sensitivity analysis that includes these additional variables.

Addressing these limitations not only highlights areas ripe for further research but also underscores the critical need for ongoing development and validation of geomechanical models. Such endeavors are paramount for advancing our collective understanding of GCS's safety and efficacy, ultimately aiding in the broader acceptance and implementation of GCS technologies as viable solutions for carbon management across a spectrum of geological scenarios.

## 7. Conclusions

This study demonstrates the technical feasibility of using a comprehensive numerical simulation framework that combines fluid flow and geomechanics to model ground deformation caused by CO<sub>2</sub> injection for storage. Although the study employed a specific geological model, the conducted sensitivity analysis enables the extension and generalization of the key findings, offering important insights into geomechanical considerations. These findings serve as valuable information for guiding future research and experimentation in this area. The main conclusions derived from this study are outlined below.

- Pressure diffusion into adjacent rocks can occur even without significant CO<sub>2</sub> migration due to the nature of pressure transmission through pore fluids. This precedes the physical movement of CO<sub>2</sub>.
- The presence of small amounts of CO<sub>2</sub> detectable in the surrounding rocks, mainly through diffusion, does not pose a leakage concern in this model, assuming the absence of fractures or other flow localization features. The limited movement of CO<sub>2</sub> into the surrounding rocks demonstrates the combined effect of the caprock's low permeability and the high capillary entry pressure, which serve as a robust containment mechanism ensuring the long-term integrity of the geological storage. Further investigation using fine-scale models is recommended to delve deeper into the mechanisms of CO<sub>2</sub> entrapment due to diffusion. The use of finer gridblocks in this model can provide a more detailed and accurate representation of the dissolution and diffusion processes.
- The study findings indicate that there is persistent ground movement resulting from pressure dissipation, which continues even after the injection period. This validates the use of high-precision instruments, such as floor tiltmeters, for monitoring CCS operations, as they are capable of accurately measuring the displacement rates associated with these activities.



- The sensitivity analysis highlights the importance of comprehensive monitoring and robust calibration of these models to effectively manage geomechanical risks associated with CO<sub>2</sub> injection. The findings suggest that rocks with higher Poisson ratios and lower Young's modulus values experience increased vertical displacements. Additionally, higher CO<sub>2</sub> injection rates and reduced shale permeabilities are associated with greater displacement magnitudes. This interplay between rock mechanical properties and operational parameters provides a basis for future research aimed at optimizing CO<sub>2</sub> storage strategies and ensuring the integrity of geological storage sites.

**Author Contributions:** Conceptualization, G.S.S., M.V.B.M., M.D., D.V., F.C.V. and K.S.; methodology, G.S.S. and M.V.B.M.; software, G.S.S. and M.V.B.M.; validation, M.D., D.V., F.C.V. and K.S.; formal analysis, G.S.S., M.V.B.M., M.D., D.V., F.C.V. and K.S.; investigation, G.S.S., M.V.B.M., M.D., D.V., F.C.V. and K.S.; resources, M.D., D.V., F.C.V. and K.S.; data curation, G.S.S. and M.V.B.M.; writing—original draft preparation, G.S.S., M.V.B.M., M.D., D.V., F.C.V. and K.S.; writing—review and editing, M.D., D.V., F.C.V. and K.S.; visualization, G.S.S., M.V.B.M., M.D., D.V., F.C.V. and K.S.; supervision, M.D., D.V., F.C.V. and K.S.; project administration, M.D., D.V., F.C.V. and K.S. All authors have read and agreed to the published version of the manuscript.

**Funding:** This research received no external funding.

**Institutional Review Board Statement:** Not applicable.

**Informed Consent Statement:** Not applicable.

**Data Availability Statement:** The data used in this study are provided within the article, and the UNISIM-I geological model is openly available at <https://www.unisim.cepetro.unicamp.br/benchmarks/en/> (accessed on 12 December 2023).

**Acknowledgments:** The authors express their gratitude to PETROBRAS for granting permission to use the data and models in this study.

**Conflicts of Interest:** The authors Gabriel Serrão Seabra and Marcos Vitor Barbosa Machado are employed by the company PETROBRAS. The remaining authors declare that the research was conducted in the absence of any commercial or financial relationships that could be construed as a potential conflict of interest.

## Nomenclature

$B_{CO_2}$	parameter for Langmuir isotherm relation, 1/kPa
$C$	Land's constant, dimensionless
$c_f$	rock compressibility, kPa <sup>-1</sup>
$D$	diffusion coefficient, cm <sup>2</sup> /s
$D_{eff}$	effective diffusion coefficient, cm <sup>2</sup> /s
$g$	acceleration due to gravity, m/s <sup>2</sup>
$H$	aquifer thickness, m
$H_i$	Henry's constant at current pressure ( $p$ ) and temperature ( $T$ ), dimensionless
$H_i^*$	Henry's constant at reference pressure ( $p^*$ ) and temperature ( $T$ ), dimensionless
$J$	Leverett J-function, dimensionless
$k$ or $k_h$	average horizontal permeability, mD [ $9.869 \times 10^{-16} \text{ m}^2$ ]
$k_v$	average vertical permeability, mD [ $9.869 \times 10^{-16} \text{ m}^2$ ]
$k_{rl}$	relative permeability, dimensionless
$L$	length of the aquifer, m
$L_w$	horizontal well length, m
$M$	mobility ratio, dimensionless
$N_j$	the total moles of mineral $j$ , gmol/m <sup>3</sup>
$N_{gv}$	characteristic time ratio for fluid to flow in the transverse direction due to gravity, dimensionless
$I$	identity tensor
$K$	stiffness tensor
$p$	pore pressure, kPa

$P_c$	CO <sub>2</sub> –brine capillary pressure, kPa
$R$	universal gas constant, 8.314 kPa·L/mol·K
$rf$	resistance factor, dimensionless
$S_{gt}$	trapped gas saturation, dimensionless
$S_{g\ max}$	maximum gas saturation, dimensionless
$T$	temperature, °C
$\Delta T$	temperature change, °C
$u$	the Darcy velocity (real velocity $\times \varphi$ ), m/s
$\mathbf{u}$	displacement vector
$y_{CO_2, g}$	molar fraction of adsorbed CO <sub>2</sub> in the gas phase, dimensionless
$Z$	global mole fraction, dimensionless
<i>Greek symbols</i>	
$\varphi$	rock porosity, fraction
$\mu_{brine}$	brine viscosity, cP [ $10^{-3}$ Pa.s]
$\rho_m$	mineral molar density, gmol/m <sup>3</sup>
$\rho$	density, kg/m <sup>3</sup>
$\tau$	tortuosity, dimensionless
$\bar{v}_i$	partial molar volume at infinite dilution, L/mol
$\omega_{CO_2}$	moles of adsorbed CO <sub>2</sub> per unit mass of rock, gmole/kg of rock
$\omega_{CO_2, max}$	maximum moles of adsorbed CO <sub>2</sub> per unit mass of rock, gmole/kg of rock
$\sigma$	stress tensor
$\varepsilon$	strain tensor
$\alpha$	Biot coefficient
$\eta$	thermoelastic coefficient

## References

1. Birol, D.F. *World Energy Outlook 2022*; IEA Publications: Paris, France, 2022.
2. Nghiem, L.; Shrivastava, V.; Kohse, B.; Hassam, M.; Yang, C. Simulation of Trapping Processes for CO<sub>2</sub> Storage in Saline Aquifers. In Proceedings of the Canadian International Petroleum Conference, Calgary, Alberta, 16–18 June 2009; Petroleum Society of Canada: Calgary, AB, Canada, 2009.
3. Han, W.S.; McPherson, B.J.; Lichtner, P.C.; Wang, F.P. Evaluation of Trapping Mechanisms in Geologic CO<sub>2</sub> Sequestration: Case Study of SACROC Northern Platform, a 35-Year CO<sub>2</sub> Injection Site. *Am. J. Sci.* **2010**, *310*, 282–324. [[CrossRef](#)]
4. Delshad, M.; Kong, X.; Tavakoli, R.; Hosseini, S.A.; Wheeler, M.F. Modeling and Simulation of Carbon Sequestration at Cranfield Incorporating New Physical Models. *Int. J. Greenh. Gas Control* **2013**, *18*, 463–473. [[CrossRef](#)]
5. Rackley, S.A. *Carbon Capture and Storage*, 2nd ed.; Butterworth-Heinemann: Cambridge, MA, USA, 2017; ISBN 978-0-12-812041-5.
6. Hovorka, S. *Optimization of Geological Environments for Carbon Dioxide Disposal in Saline Aquifers in the United States (Part One)*; University of Texas: Austin, TX, USA, 2008; p. 990445.
7. Bump, A.P.; Bakhshian, S.; Ni, H.; Hovorka, S.D.; Olariu, M.I.; Dunlap, D.; Hosseini, S.A.; Meckel, T.A. Composite Confining Systems: Rethinking Geologic Seals for Permanent CO<sub>2</sub> Sequestration. *Int. J. Greenh. Gas Control* **2023**, *126*, 103908. [[CrossRef](#)]
8. Duan, Z.; Sun, R. An Improved Model Calculating CO<sub>2</sub> Solubility in Pure Water and Aqueous NaCl Solutions from 273 to 533 K and from 0 to 2000 Bar. *Chem. Geol.* **2003**, *193*, 257–271. [[CrossRef](#)]
9. Portier, S.; Rochelle, C. Modelling CO<sub>2</sub> Solubility in Pure Water and NaCl-Type Waters from 0 to 300 °C and from 1 to 300 Bar. *Chem. Geol.* **2005**, *217*, 187–199. [[CrossRef](#)]
10. Farajzadeh, R.; Zitha, P.L.J.; Bruining, J. Enhanced Mass Transfer of CO<sub>2</sub> into Water: Experiment and Modeling. *Ind. Eng. Chem. Res.* **2009**, *48*, 6423–6431. [[CrossRef](#)]
11. Neufeld, J.A.; Hesse, M.A.; Riaz, A.; Hallworth, M.A.; Tchelepi, H.A.; Huppert, H.E. Convective Dissolution of Carbon Dioxide in Saline Aquifers. *Geophys. Res. Lett.* **2010**, *37*, 22. [[CrossRef](#)]
12. Taheri, A.; Torsæter, O.; Lindeberg, E.; Hadia, N.J.; Wessel-Berg, D. Effect of Convective Mixing Process on Storage of CO<sub>2</sub> in Saline Aquifers with Layered Permeability. *Adv. Chem. Res.* **2021**, *3*, 1–21. [[CrossRef](#)]
13. Amarasingham, W.; Farzaneh, S.; Fjelde, I.; Sohrabi, M.; Guo, Y. A Visual Investigation of CO<sub>2</sub> Convective Mixing in Water and Oil at the Pore Scale Using a Micromodel Apparatus at Reservoir Conditions. *Gases* **2021**, *1*, 53–67. [[CrossRef](#)]
14. Elenius, M.T.; Voskov, D.V.; Tchelepi, H.A. Interactions between Gravity Currents and Convective Dissolution. *Adv. Water Resour.* **2015**, *83*, 77–88. [[CrossRef](#)]
15. Spiteri, E.J.; Juanes, R.; Blunt, M.J.; Orr, F.M. Relative Permeability Hysteresis: Trapping Models and Application to Geological CO<sub>2</sub> Sequestration. In Proceedings of the All Days, SPE Annual Technical Conference and Exhibition, Dallas, TX, USA, 9–12 October 2005; SPE: Dallas, TX, USA, 2005; p. SPE-96448-MS.
16. Nghiem, L.; Yang, C.; Shrivastava, V.; Kohse, B.; Hassam, M.; Card, C. Risk Mitigation through the Optimization of Residual Gas and Solubility Trapping for CO<sub>2</sub> Storage in Saline Aquifers. *Energy Procedia* **2009**, *1*, 3015–3022. [[CrossRef](#)]
17. Qi, R.; Laforce, T.; Blunt, M. Design of Carbon Dioxide Storage in Aquifers. *Int. J. Greenh. Gas Control* **2009**, *3*, 195–205. [[CrossRef](#)]

18. Lyu, X.; Voskov, D. Advanced Modeling of Enhanced CO<sub>2</sub> Dissolution Trapping in Saline Aquifers. *Int. J. Greenh. Gas Control* **2023**, *127*, 103907. [[CrossRef](#)]
19. Xu, T.; Yue, G.; Wang, F.; Liu, N. Using Natural CO<sub>2</sub> Reservoir to Constrain Geochemical Models for CO<sub>2</sub> Geological Sequestration. *Appl. Geochem.* **2014**, *43*, 22–34. [[CrossRef](#)]
20. Gunter, W.D.; Bachu, S.; Benson, S. The Role of Hydrogeological and Geochemical Trapping in Sedimentary Basins for Secure Geological Storage of Carbon Dioxide. *Geol. Soc. Lond. Spec. Publ.* **2004**, *233*, 129–145. [[CrossRef](#)]
21. Song, Y.; Jun, S.; Na, Y.; Kim, K.; Jang, Y.; Wang, J. Geomechanical Challenges during Geological CO<sub>2</sub> Storage: A Review. *Chem. Eng. J.* **2023**, *456*, 140968. [[CrossRef](#)]
22. Wouters, M.; Hanssen, R.F.; Govers, R. Using PS-InSAR Observations to Detect Aseismic Fault Slip in the Seismically Active Groningen Gas Field. In Proceedings of the AGU Fall Meeting 2021, New Orleans, LA, USA, 13–17 December 2021.
23. Nagel, N.B. Compaction and Subsidence Issues within the Petroleum Industry: From Wilmington to Ekofisk and Beyond. *Phys. Chem. Earth Part A Solid Earth Geod.* **2001**, *26*, 3–14. [[CrossRef](#)]
24. Morris, J.P.; Hao, Y.; Foxall, W.; McNab, W. In Salah CO<sub>2</sub> Storage JIP: Hydromechanical Simulations of Surface Uplift Due to CO<sub>2</sub> Injection at In Salah. *Energy Procedia* **2011**, *4*, 3269–3275. [[CrossRef](#)]
25. Vilarrasa, V.; Makhnenko, R.Y.; Rutqvist, J. Field and Laboratory Studies of Geomechanical Response to the Injection of CO<sub>2</sub>. In *Science of Carbon Storage in Deep Saline Formations*; Elsevier: Amsterdam, The Netherlands, 2019; pp. 209–236, ISBN 978-0-12-812752-0.
26. Gharbi, O.; Bijeljic, B.; Boek, E.; Blunt, M.J. Changes in Pore Structure and Connectivity Induced by CO<sub>2</sub> Injection in Carbonates: A Combined Pore-Scale Approach. *Energy Procedia* **2013**, *37*, 5367–5378. [[CrossRef](#)]
27. Snippe, J.; Berg, S.; Ganga, K.; Brussee, N.; Gdanski, R. Experimental and Numerical Investigation of Wormholing during CO<sub>2</sub> Storage and Water Alternating Gas Injection. *Int. J. Greenh. Gas Control.* **2020**, *94*, 102901. [[CrossRef](#)]
28. Bacci, G.; Korre, A.; Durucan, S. Experimental Investigation into Salt Precipitation during CO<sub>2</sub> Injection in Saline Aquifers. *Energy Procedia* **2011**, *4*, 4450–4456. [[CrossRef](#)]
29. Guyant, E.; Han, W.S.; Kim, K.-Y.; Park, M.-H.; Kim, B.-Y. Salt Precipitation and CO<sub>2</sub>/Brine Flow Distribution under Different Injection Well Completions. *Int. J. Greenh. Gas Control.* **2015**, *37*, 299–310. [[CrossRef](#)]
30. Ahusborde, E.; Amaziane, B.; De Hoop, S.; El Ossmani, M.; Flauraud, E.; Hamon, F.P.; Kern, M.; Socié, A.; Su, D.; Mayer, K.U.; et al. A Benchmark Study on Reactive Two-Phase Flow in Porous Media: Part II—Results and Discussion. *Comput. Geosci.* **2024**, *1*–18. [[CrossRef](#)]
31. De Hoop, S.; Voskov, D.; Ahusborde, E.; Amaziane, B.; Kern, M. A Benchmark Study on Reactive Two-Phase Flow in Porous Media: Part I—Model Description. *Comput. Geosci.* **2024**, *28*, 175–189. [[CrossRef](#)]
32. Kim, K.; Vilarrasa, V.; Makhnenko, R. CO<sub>2</sub> Injection Effect on Geomechanical and Flow Properties of Calcite-Rich Reservoirs. *Fluids* **2018**, *3*, 66. [[CrossRef](#)]
33. Harvey, S.; O'Brien, S.; Minisini, S.; Oates, S.; Braim, M. Quest CCS Facility: Microseismic System Monitoring and Observations. In Proceedings of the 15th Greenhouse Gas Control Technologies Conference, Virtual, 15–18 March 2021. [[CrossRef](#)]
34. Braim, M.; Bowman, S.; Waggott, B. Stress Evolution During CO<sub>2</sub> Storage—A Case for Long-Term Monitoring. *First Break* **2023**, *41*, 43–47. [[CrossRef](#)]
35. Verma, Y.; Vishal, V.; Ranjith, P.G. Sensitivity Analysis of Geomechanical Constraints in CO<sub>2</sub> Storage to Screen Potential Sites in Deep Saline Aquifers. *Front. Clim.* **2021**, *3*, 720959. [[CrossRef](#)]
36. Tang, M.; Ju, X.; Durlifsky, L.J. Deep-Learning-Based Coupled Flow-Geomechanics Surrogate Model for CO<sub>2</sub> Sequestration. *arXiv* **2021**, arXiv:2105.01334. [[CrossRef](#)]
37. Zheng, F.; Jha, B.; Jafarpour, B. Controlled CO<sub>2</sub> Injection into Storage Reservoirs to Minimize Geomechanical Risks under Geologic Uncertainty. In Proceedings of the SPE Annual Technical Conference and Exhibition, San Antonio, TX, USA, 17 October 2023; p. D021S020R005. [[CrossRef](#)]
38. AL-Ameri, W.A.; Abdulraheem, A.; Mahmoud, M. Long-Term Effects of CO<sub>2</sub> Sequestration on Rock Mechanical Properties. *J. Energy Resour. Technol.* **2016**, *138*, 012201. [[CrossRef](#)]
39. He, X.; Zhu, W.; AlSinan, M.; Kwak, H.; Hoteit, H. CO<sub>2</sub> Storage Capacity Prediction In Deep Saline Aquifers: Uncertainty and Global Sensitivity Analysis. In Proceedings of the International Petroleum Technology Conference, Riyadh, Saudi Arabia, 22 February 2022; p. D021S044R003. [[CrossRef](#)]
40. Davis, E.; Wright, C.; Demetrius, S.; Choi, J.; Craley, G. Precise Tiltmeter Subsidence Monitoring Enhances Reservoir Management. In Proceedings of the All Days, SPE/AAPG Western Regional Meeting, Long Beach, CA, USA, 19 June 2000; p. SPE-62577-MS.
41. Bouquet, S.; Frey, J.; Malinouskaya, I.; Estublier, A.; Fournio, A. Evaluation of Surface Movement Observability and Optimization of the Monitoring Plan through Conceptual and Coupled Flow-Geomechanics Models. Examples of Carbonate and Sandstone Reservoirs in CCS Context. In Proceedings of the 16th Greenhouse Gas Control Technologies Conference (GHGT-16), Lyon, France, 23–24 October 2022. [[CrossRef](#)]
42. Shi, J.-Q.; Smith, J.; Durucan, S.; Korre, A. A Coupled Reservoir Simulation-Geomechanical Modelling Study of the CO<sub>2</sub> Injection-Induced Ground Surface Uplift Observed at Krechba, in Salah. *Energy Procedia* **2013**, *37*, 3719–3726. [[CrossRef](#)]
43. Zhang, T.; Zhang, W.; Yang, R.; Gao, H.; Cao, D. Analysis of Available Conditions for InSAR Surface Deformation Monitoring in CCS Projects. *Energies* **2022**, *15*, 672. [[CrossRef](#)]
44. Ervine, C. Directive 2004/39/Ec of the European Parliament and of the Council of 21 April 2004. In *Core Statutes on Company Law*; Macmillan Education: London, UK, 2015; pp. 757–759, ISBN 978-1-137-54506-0.

45. Bump, A.P.; Hovorka, S.D. Fetch-Trap Pairs: Exploring Definition of Carbon Storage Prospects to Increase Capacity and Flexibility in Areas with Competing Uses. *Int. J. Greenh. Gas Control* **2023**, *122*, 103817. [CrossRef]
46. Buscheck, T.A.; Sun, Y.; Chen, M.; Hao, Y.; Wolery, T.J.; Bourcier, W.L.; Court, B.; Celia, M.A.; Julio Friedmann, S.; Aines, R.D. Active CO<sub>2</sub> Reservoir Management for Carbon Storage: Analysis of Operational Strategies to Relieve Pressure Buildup and Improve Injectivity. *Int. J. Greenh. Gas Control* **2012**, *6*, 230–245. [CrossRef]
47. Kim, M.; Kwon, S.; Ji, M.; Shin, H.; Min, B. Multi-Lateral Horizontal Well with Dual-Tubing System to Improve CO<sub>2</sub> Storage Security and Reduce CCS Cost. *Appl. Energy* **2023**, *330*, 120368. [CrossRef]
48. Singh, M.; Chaudhuri, A.; Chu, S.P.; Stauffer, P.H.; Pawar, R.J. Analysis of Evolving Capillary Transition, Gravitational Fingering, and Dissolution Trapping of CO<sub>2</sub> in Deep Saline Aquifers during Continuous Injection of Supercritical CO<sub>2</sub>. *Int. J. Greenh. Gas Control* **2019**, *82*, 281–297. [CrossRef]
49. Lei, T.; Luo, K.H. Pore-Scale Simulation of Miscible Viscous Fingering with Dissolution Reaction in Porous Media. *Phys. Fluids* **2021**, *33*, 034134. [CrossRef]
50. Machado, M.V.B.; Delshad, M.; Sepehrnoori, K. Injectivity Assessment for CCS Field-Scale Projects with Considerations of Salt Deposition, Mineral Dissolution, Fines Migration, Hydrate Formation, and Non-Darcy Flow. *Fuel* **2023**, *353*, 129148. [CrossRef]
51. Gholami, R.; Raza, A.; Iglauer, S. Leakage Risk Assessment of a CO<sub>2</sub> Storage Site: A Review. *Earth-Sci. Rev.* **2021**, *223*, 103849. [CrossRef]
52. Farshidi, S.F.; Fan, Y.; Durlinsky, L.J.; Tchepeli, H.A. Chemical Reaction Modeling in a Compositional Reservoir-Simulation Framework. In Proceedings of the All Days, SPE Reservoir Simulation Symposium, The Woodlands, TX, USA, 18 February 2013; p. SPE-163677-MS.
53. Machado, M.V.B.; Khanal, A.; Delshad, M. Unveiling the Essential Parameters Driving Mineral Reactions during CO<sub>2</sub> Storage in Carbonate Aquifers through Proxy Models. *Appl. Sci.* **2024**, *14*, 1465. [CrossRef]
54. Avansi, G.D.; Schiozer, D.J. UNISIM-I: Synthetic Model for Reservoir Development and Management Applications. *Int. J. Model. Simul. Pet. Ind.* **2015**, *9*, 21–30.
55. Gercek, H. Poisson's Ratio Values for Rocks. *Int. J. Rock Mech. Min. Sci.* **2007**, *44*, 1–13. [CrossRef]
56. Molina, O.; Vilarrasa, V.; Zeidouni, M. Geologic Carbon Storage for Shale Gas Recovery. *Energy Procedia* **2017**, *114*, 5748–5760. [CrossRef]
57. Energies | Free Full-Text | Periodic CO<sub>2</sub> Injection for Improved Storage Capacity and Pressure Management under Intermittent CO<sub>2</sub> Supply. Available online: <https://www.mdpi.com/1996-1073/15/2/566> (accessed on 1 March 2024).
58. Kuk, M.; Kuk, E.; Janiga, D.; Wojnarowski, P.; Stopa, J. Optimization Wells Placement Policy for Enhanced CO<sub>2</sub> Storage Capacity in Mature Oil Reservoirs. *Energies* **2020**, *13*, 4054. [CrossRef]
59. Machado, M.V.B.; Delshad, M.; Sepehrnoori, K. Potential Benefits of Horizontal Wells for CO<sub>2</sub> Injection to Enhance Storage Security and Reduce Leakage Risks. *Appl. Sci.* **2023**, *13*, 12830. [CrossRef]
60. Bennion, D.B.; Bachu, S. Drainage and Imbibition Relative Permeability Relationships for Supercritical CO<sub>2</sub>/Brine and H<sub>2</sub>S/Brine Systems in Intergranular Sandstone, Carbonate, Shale, and Anhydrite Rocks. *SPE Reserv. Eval. Eng.* **2008**, *11*, 487–496. [CrossRef]
61. Abdoulghafour, H.; Sarmadivaleh, M.; Hauge, L.P.; Fernø, M.; Iglauer, S. Capillary Pressure Characteristics of CO<sub>2</sub>-Brine-Sandstone Systems. *Int. J. Greenh. Gas Control.* **2020**, *94*, 102876. [CrossRef]
62. Bennion, D.B.; Bachu, S. Permeability and Relative Permeability Measurements at Reservoir Conditions for CO<sub>2</sub>-Water Systems in Ultralow-Permeability Confining Caprocks. In Proceedings of the All Days, EUROPEC/EAGE Conference and Exhibition, London, UK, 11 June 2007; p. SPE-106995-MS.
63. CMG. GEM, Compositional & Unconventional Simulator, (version 2023.30); Windows, CMG: Calgary, AB, Canada, 2023.
64. Machado, M.V.B.; Delshad, M.; Sepehrnoori, K. A Practical and Innovative Workflow to Support the Numerical Simulation of CO<sub>2</sub> Storage in Large Field-Scale Models. *SPE Reserv. Eval. Eng.* **2023**, *26*, 1541–1552. [CrossRef]
65. Balhoff, M. *An Introduction to Multiphase, Multicomponent Reservoir Simulation*; Developments in Petroleum Science; Elsevier: Amsterdam, The Netherlands, 2022; ISBN 978-0-323-99235-0.
66. Machado, M.V.B. *Numerical Petroleum Reservoir Modeling: Integrated Simulation Practice*, 1st ed.; PETROBRAS: Rio de Janeiro, RJ, Brazil, 2023; ISBN 9786588763070. (In Portuguese)
67. Li, Y.-K.; Nghiem, L.X. Phase Equilibria of Oil, Gas and Water/Brine Mixtures from a Cubic Equation of State and Henry's Law. *Can. J. Chem. Eng.* **1986**, *64*, 486–496. [CrossRef]
68. Bakker, R.J. Package FLUIDS 1. Computer Programs for Analysis of Fluid Inclusion Data and for Modelling Bulk Fluid Properties. *Chem. Geol.* **2003**, *194*, 3–23. [CrossRef]
69. Rezk, M.G.; Foroozesh, J.; Abdulrahman, A.; Gholinezhad, J. CO<sub>2</sub> Diffusion and Dispersion in Porous Media: Review of Advances in Experimental Measurements and Mathematical Models. *Energy Fuels* **2022**, *36*, 133–155. [CrossRef]
70. Busch, A.; Alles, S.; Gensterblum, Y.; Prinz, D.; Dewhurst, D.N.; Raven, M.D.; Stanjek, H.; Krooss, B.M. Carbon Dioxide Storage Potential of Shales. *Int. J. Greenh. Gas Control.* **2008**, *2*, 297–308. [CrossRef]
71. Montegrossi, G.; Cantucci, B.; Piochi, M.; Fusi, L.; Misnan, M.S.; Rashidi, M.R.A.; Abu Bakar, Z.A.; Tuan Harith, Z.Z.; Bahri, N.H.S.; Hashim, N. CO<sub>2</sub> Reaction-Diffusion Experiments in Shales and Carbonates. *Minerals* **2022**, *13*, 56. [CrossRef]
72. Land, C.S. Calculation of Imbibition Relative Permeability for Two- and Three-Phase Flow from Rock Properties. *Soc. Pet. Eng. J.* **1968**, *8*, 149–156. [CrossRef]

73. Carlson, F.M. Simulation of Relative Permeability Hysteresis to the Nonwetting Phase. In Proceedings of the SPE Annual Technical Conference and Exhibition, San Antonio, TX, USA, 4 October 1981; p. SPE-10157-MS.
74. Burnside, N.M.; Naylor, M. Review and Implications of Relative Permeability of CO<sub>2</sub>/Brine Systems and Residual Trapping of CO<sub>2</sub>. *Int. J. Greenh. Gas Control* **2014**, *23*, 1–11. [[CrossRef](#)]
75. Lima, C.; Nascimento, E.; Assumpção, M. Stress Orientations in Brazilian Sedimentary Basins from Breakout Analysis: Implications for Force Models in the South American Plate. *Geophys. J. Int.* **1997**, *130*, 112–124. [[CrossRef](#)]
76. Assumpção, M. Seismicity and Stresses in the Brazilian Passive Margin. *Bull. Seismol. Soc. Am.* **1998**, *88*, 160–169. [[CrossRef](#)]
77. Bizzo, Y.F. Evaluation of the Effects of Fluid and Rock Properties on Geomechanical Simulations of Reservoirs from the Namorado Field. Master's Thesis, Pontifical Catholic University of Rio de Janeiro, Rio de Janeiro, Brazil, 2017.
78. Lima, R.O.; do Nascimento Guimarães, L.J.; Pereira, L.C. Evaluating Geomechanical Effects Related to the Production of a Brazilian Reservoir. *J. Petrol. Explor. Prod. Technol.* **2021**, *11*, 2661–2678. [[CrossRef](#)]
79. Bjørnarå, T.I.; Aker, E.; Cuisiat, F.; Skurtveit, E. Modeling CO<sub>2</sub> Storage Using Coupled Reservoir-Geomechanical Analysis. In Proceedings of the COMSOL Conference, Paris, France, 17–19 November 2010.
80. Kim, J.; Tchelepi, H.A.; Juanes, R. Stability, Accuracy, and Efficiency of Sequential Methods for Coupled Flow and Geomechanics. *SPE J.* **2011**, *16*, 249–262. [[CrossRef](#)]
81. Garipov, T.T.; Hui, M. Simulation of Coupled Geomechanics and Multiphase Flow in Naturally Fractured Reservoirs. In Proceedings of the 52nd U.S. Rock Mechanics/Geomechanics Symposium, Seattle, DC, USA, 17 June 2018; p. ARMA-2018-1230.
82. Tran, D.; Nghiem, L.; Settari, A. New Iterative Coupling Between a Reservoir Simulator and a Geomechanics Module. *SPE J.* **2004**, *9*, 362–369. [[CrossRef](#)]
83. Gasda, S.E.; Wangen, M.; Bjørnarå, T.I.; Elenius, M.T. Investigation of Caprock Integrity Due to Pressure Build-up During High-Volume Injection into the Utsira Formation. *Energy Procedia* **2017**, *114*, 3157–3166. [[CrossRef](#)]
84. Zheng, X.; Espinoza, D.N.; Vandamme, M.; Pereira, J.-M. CO<sub>2</sub> Plume and Pressure Monitoring through Pressure Sensors above the Caprock. *Int. J. Greenh. Gas Control* **2022**, *117*, 103660. [[CrossRef](#)]
85. Currenti, G.; Cantucci, B.; Montegrossi, G.; Napoli, R.; Misnan, M.S.; Rashidi, M.R.A.; Abu Bakar, Z.A.; Harith, Z.Z.T.; Bahri, N.H.S.; Hashim, N. CO<sub>2</sub> Leakage Scenarios in Shale Overburden. *Minerals* **2023**, *13*, 1016. [[CrossRef](#)]
86. Hosa, A.; Esentia, M.; Stewart, J.; Haszeldine, S. Injection of CO<sub>2</sub> into Saline Formations: Benchmarking Worldwide Projects. *Chem. Eng. Res. Des.* **2011**, *89*, 1855–1864. [[CrossRef](#)]
87. Metz, B. (Ed.) *IPCC Special Report on Carbon Dioxide Capture and Storage*; Cambridge University Press, for the Intergovernmental Panel on Climate Change: Cambridge, UK, 2005; ISBN 978-0-521-86643-9.

**Disclaimer/Publisher's Note:** The statements, opinions and data contained in all publications are solely those of the individual author(s) and contributor(s) and not of MDPI and/or the editor(s). MDPI and/or the editor(s) disclaim responsibility for any injury to people or property resulting from any ideas, methods, instructions or products referred to in the content.